

Article

Basin-Scale Streamflow Projections for Greater Pamba River Basin, India Integrating GCM Ensemble Modelling and Flow Accumulation-Weighted LULC Overlay in Deep Learning Environment

Arathy Nair Geetha Raveendran Nair ^{1,2}, Shamla Dilama Shamsudeen ^{1,2}, Meera Geetha Mohan ^{1,2} and Adarsh Sankaran ^{1,2,*} 

¹ Thangal Kunju Musaliar College of Engineering, Kollam 691005, Kerala, India; 212027@tkmce.ac.in (A.N.G.R.N.); meeragm@tkmce.ac.in (M.G.M.)

² Department of Civil Engineering, Thangal Kunju Musaliar College of Engineering, APJ Abdul Kalam Technological University, Kollam 695016, Kerala, India

* Correspondence: adarsh1982@tkmce.ac.in

Abstract: Accurate prediction of future streamflow in flood-prone regions is crucial for effective flood management and disaster mitigation. This study presents an innovative approach for streamflow projections in deep learning (DL) environment by integrating the quantitative Land-Use Land-Cover (LULC) overlaid with flow accumulation values and the various Global Climate Model (GCM) simulated data. Firstly, the Long Short Term Memory (LSTM) model was developed for the streamflow prediction of Greater Pamba River Basin (GPRB) in Kerala, India for 1985 to 2015 period, considering the climatic inputs. Then, the flow accumulation-weighted LULC integration was considered in modelling, which substantially improves the accuracy of streamflow predictions including the extremes of all the three stations, as the model accounts for the geographical variety of land cover types towards the streamflow at the sub-basin outlets. Subsequently, Reliability Ensemble Averaging (REA) technique was used to create an ensemble of three candidate GCM products to illustrate the spectrum of uncertainty associated with climate projections. Future LULC changes are accounted in regional scale based on the sub-basin approach by means of Cellular-Automata Markov Model and used for integrating with the climatic indices. The basin-scale streamflow projection is done under three climate scenarios of SSP126, SSP245 and SSP585 respectively for lowest, moderate and highest emission conditions. This work is a novel approach of integrating quantified LULC with flow accumulation and other climatic inputs in a DL environment against the conventional techniques of hydrological modelling. The DL model can adapt and account for shifting hydrological responses induced by changes in climatic and LULC inputs. The integration of flow accumulation with changes in LULC was successful in capturing the flow dynamics in long-term. It also identifies regions that are more likely to experience increased flooding in the near future under changing climate scenarios and supports decision-making for sustainable water management of the Greater Pamba Basin which was the worst affected region in Kerala during the mega floods of 2018.

Keywords: LULC; Global Climate Model; Reliability Ensemble Averaging; Long Short Term Memory



Citation: Geetha Raveendran Nair, A.N.; Shamsudeen, S.D.; Mohan, M.G.; Sankaran, A. Basin-Scale Streamflow Projections for Greater Pamba River Basin, India Integrating GCM Ensemble Modelling and Flow Accumulation-Weighted LULC Overlay in Deep Learning Environment. *Sustainability* **2023**, *15*, 14148. <https://doi.org/10.3390/su151914148>

Academic Editor: Subhasis Giri

Received: 6 July 2023

Revised: 14 September 2023

Accepted: 20 September 2023

Published: 25 September 2023



Copyright: © 2023 by the authors. Licensee MDPI, Basel, Switzerland. This article is an open access article distributed under the terms and conditions of the Creative Commons Attribution (CC BY) license (<https://creativecommons.org/licenses/by/4.0/>).

1. Introduction

The sustainable management of water resources is a vital component of combating the challenges posed by climate change and safeguarding the well-being of communities and ecosystems. Effective water resource planning and management depend heavily on streamflow forecasts, which offer insights into future water availability and trends. Increased streamflow pattern variability is encouraged by changes in land use within the river basins [1–4]. The modification of the land and its associated resources has through

time evolved into one of the pressing problems presently gaining attention on a world-wide scale and is now vital to sustainability and environmental preservation [5]. The consequences on streamflow variability have been further exacerbated by increased land use/land cover (LULC) changes brought on by rapid population growth and the concomitant socio-economic development from several viewpoints [6,7]. This manifests the necessity of future LULC projection for streamflow forecast. It aids in capturing changes in evapotranspiration, land surface features, surface runoff, and land management practices [8,9].

In order to identify and simulate LULC changes, a variety of techniques are employed, including mathematical equations, system dynamics, statistics, expert systems, evolution, cellular, and hybrid models [10]. However, hybrid models are the most often utilized techniques. Cellular Automata (CA) and Markov models are combined to create CA-Markov models, which have been deemed ideal for modelling LULC changes because they can account for both the spatial and temporal aspects of LULC dynamics [11,12].

Streamflow patterns are impacted by surface runoff, infiltration rates, and evapotranspiration rates, which are in turn influenced by vegetation cover, impervious surfaces, and soil characteristics. Taking into consideration the crucial role of LULC features in hydrological processes, the goal is to improve the accuracy and reliability of future streamflow estimates by explicitly accounting for the effects of climate change. The spatially explicit effect of LULC features and its influence on flow accumulation ranges are frequently ignored by traditional streamflow projection techniques, which can result in forecasts that may be incorrect. In this study, the proposed method includes a flow accumulation-weighted LULC overlay technique to get over this drawback. In hydrological models that replicate the water balance within a basin, flow accumulation is frequently employed as an input parameter [12]. The basin's geographical heterogeneity of hydrological processes is captured by allocating weights to various land cover classes based on their contributions to streamflow generation. This technique recognizes that not all types of land cover exert the same influence on streamflow and that their impact should be fully accounted for to enhance prediction accuracy. The aforementioned technique is consistent with the notion of runoff coefficients, which are the widely recognized hydrological parameters employed to measure the percentage of precipitation that converts into runoff within certain land cover classifications. By allocating suitable flow accumulation weightage to distinct land cover categories, the model can accurately simulate the diverse hydrological reactions observed throughout the basin, hence enhancing the accuracy of streamflow forecasts.

In addition to the anthropogenic causes, natural variables such as climate change have also had an impact on the streamflow variability [13–16]. Climate change has far-reaching ramifications in a way that it modifies precipitation timing, magnitude, and distribution, as well as evapotranspiration rates and general hydrological patterns. Therefore, the influence of climate on streamflow should be seen and measured on multiple timescales. There are a lot of studies incorporating significant climate models for streamflow projection [17,18]. Climate models project temperature rises and changes on the spatio-temporal patterns of precipitation occurrences and amounts [19,20] globally for the upcoming century. This intricate interplay between rising temperatures and precipitation dynamics holds substantial implications for hydrological processes and water resource management. Recognizing this interaction is pivotal for comprehending the multifaceted consequences of climate change on hydrological systems.

A combination of General Circulation Models (GCMs) and hydrological models is frequently used to forecast the effects of climate change on hydrological catchments [21,22]. The GCMs are thought to be the best models for analyzing the physical and dynamical behavior of the atmospheric system [23,24]. GCMs use various modelling techniques, physical representations of climatic processes, and geographic resolutions. These variances may cause significant divergence of climatic variables, such as precipitation and temperature. The possibility to include a wider variety of potential future climate circumstances is raised by developing a multi GCM ensemble, which captures a wider range of model

variations [24–27]. This ensemble framework, carried out using the technique of Reliability Ensemble Averaging (REA), allows for a thorough examination of streamflow estimates under various climate change scenarios [28]. Here, we employed an ensemble of 3 down-scaled Coupled Model Intercomparison Project 6 (CMIP6) datasets and the basin-scale streamflow projection is done under three climate Shared Socio-economic Pathway (SSP) scenarios of SSP126, SSP245 and SSP585 respectively for lowest, moderate and highest emission conditions.

In this work, we adopt a unique approach by applying a Deep Learning (DL) model for streamflow forecast, with the goal of mitigating the uncertainties associated with typical hydrological models. While hydrological models have been widely used to estimate streamflow based on climate change and LULC data, they frequently incorporate simplifications and assumptions that inject uncertainty into the modelling process. Deep learning models, on the other hand, provide the benefit of data-driven learning as well as the capacity to extract complicated spatial and temporal patterns directly from input data [29]. We harness the power of reinforcement neural networks to extract meaningful relationships and patterns by training a deep learning model of Long-Short Term Memory (LSTM) on integrated climate, LULC, and historical streamflow datasets, resulting in a more accurate and reliable streamflow projection framework. By avoiding the constraints and uncertainties of standard hydrological models, deep learning offers up new paths for streamflow prediction, improving accuracy and decreasing reliance on model assumptions [29].

Understanding the future streamflow dynamics is crucial in the context of the Greater Pamba River Basin (GPRB) in India, given that it was the area most severely damaged by the Great Floods of 2018 and has significant ecological value. The study's findings have important implications for water resource managers, politicians, and stakeholders involved in the GPRB's long-term development. This technique provides an in-depth understanding of future streamflow dynamics in the context of climate change and land use dynamics by amalgamating GCM ensemble modelling, flow accumulation-weighted LULC overlay, and a deep learning environment. These discoveries may be used to improve adaptive water management techniques, climate change adaptation plans, and resilient water allocation policies, assuring the long-term usage of water resources in the face of changing environmental circumstances.

Overall, this study delivers a substantial addition to the field by outpacing the drawbacks of current hydrological models with a cutting-edge method for projecting streamflow. We present an extensive approach capable of capturing the spatial and temporal extents of LULC, improving the accuracy and applicability of streamflow predictions in a variety of land covers by combining flow accumulation and weighted LULC overlay inside an LSTM framework.

In subsequent sections of this paper, we delve into the data sources, methodology, and implementation details of our approach. We present the results of our analysis, discuss the implications of incorporating GCM ensemble modelling and flow accumulation-weighted LULC overlay into streamflow projections, and highlight potential avenues for future research and refinement. With this study, we aim to contribute to the growing body of knowledge on integrated water resources management, providing valuable guidance for decision-making and sustainable development in the Greater Pamba River Basin, India, and beyond.

2. Materials and Methods

2.1. Study Area

The considered study area, Greater Pamba River Basin (GPRB) [30] holds significant socio-economic and cultural importance within the state of Kerala, located in the southwestern region of India. It encompasses the entirety of the land that is drained by the Pamba, Manimala, and Achankovil rivers. Among the collection of 44 rivers, the river Pamba holds the distinction of being the third longest river in the state. The Pamba River has its source at the Pulachimalai hill located in the Peerumedu plateau of the Idukki District in the Western

Ghats. It originates at an elevation of 1650 m above sea level. The river traverses through various regions in the Pathanamthitta and Alappuzha districts, including Kuttanad, which is a significant centre for rice cultivation. Finally, the Pamba River empties into the Vembanad Lake. The whole basin of GPRB extends over an area of around 4500 sq. km with the entire catchment area limited to Kerala state and is bounded on the east by Western Ghats and on the west by Arabian Sea (Figure 1). The precipitation pattern within the GPRB displays noticeable seasonal fluctuations. The geographical area undergoes a significant monsoon period spanning from June to September, which is distinguished by substantial precipitation caused by the southwest monsoon. On the other hand, the inter-annual precipitation pattern exhibits fluctuations in annual precipitation amounts, which are impacted by climatic phenomena like El Niño and La Niña events. These phenomena can result in occasional departures from the normal long-term precipitation levels. In elevated regions, the rivers exhibit dendritic and trellis drainage patterns. Upon crossing the coastal plains, the rivers exhibit a northward trajectory and converge with the Vembanad Lake at Pallathuruthy, located in close proximity to Alappuzha. The northward movement observed in the lowlands can be attributed to the accumulation of sediment in the water body, along with a northward inclination that occurred throughout the Late Pleistocene to Early Holocene period. The mean annual streamflow of this basin is around 3423.7 hm³ (Envis Centre, Ministry of Environment & Forest, Govt. of India). This basin normally has its worst flooding during the monsoon season, especially in August and September when strong and persistent rain causes the river to breach its banks. These floods may significantly hinder disaster relief and management operations by causing extensive harm to the houses, infrastructure, and crops in the region. Kerala has recently undergone disastrous floods, particularly in 2018, which was one of the worst floods in the history of the state, showing the area's susceptibility to such occurrences. Table 1 provides a concise overview of the statistical characterizations of monsoonal precipitation and temperature (monsoon months of June to September) of selected grid points of GPRB for a time range of 1985 to 2015. This analysis is crucial as these meteorological factors play a pivotal role in exacerbating the flood risk in this region. The best fit distributions for each of these parameters are determined from a pool of distributions (Gamma, Beta, Exponential, Normal, Weibull, Generalized Extreme Value (GEV), Log Pearson Type III and Log-logistic Distributions), using the python platform. The error measures of Bayesian Information Criterion (BIC) and Kolmogorov-Smirnov test are used to assess the fit of the distribution, considering the model complexity and the distribution of data. Figures 2 and 3 represents the inter-annual variability of parameters for the selected locations. In the Figure 2, (a) represents the grid location with latitude/longitude value of 9.375/76.375, (b) as that of 9.375/76.625, (c) as 9.375/76.875, (d) 9.625/76.875, (e) as 9.375/77.125 and (f) as 9.125/77.125.

Table 1. The statistical characteristics of monsoonal daily precipitation and temperature (June to September months of the years 1985 to 2015) prevailing in the selected grid points of GPRB.

Grid Locations	Parameters	Maxi. Value	Min. Value	Standard Deviation	Coefficient of Variation	Best Fit Distribution
76.375/9.375	Precipitation	201.23	0	17.35	1.44	GEV
	Maximum Temperature	31.02	25.11	0.796	0.03	Normal
	Minimum Temperature	28.63	23.74	0.729	0.02	Gamma

Table 1. Cont.

Grid Locations	Parameters	Maxi. Value	Min. Value	Standard Deviation	Coefficient of Variation	Best Fit Distribution
76.625/9.375	Precipitation	201.19	0	14.75	1.51	Log-Logistic
	Maximum Temperature	33.7	22.69	1.23	0.04	Gamma
	Minimum Temperature	24.5	18.72	0.722	0.03	Normal
76.875/9.375	Precipitation	200.36	0	14.8	2.09	GEV
	Maximum Temperature	33.7	23.65	1.23	0.04	Normal
	Minimum Temperature	24.67	21.36	0.62	0.03	Normal
76.875/9.625	Precipitation	210.36	0	11.26	1.9	Log-Pearson Type III
	Maximum Temperature	36.69	26.54	1.51	0.03	Normal
	Minimum Temperature	27.43	21.99	0.74	0.04	Gamma
77.125/9.375	Precipitation	196.35	0	14.61	2.03	GEV
	Maximum Temperature	33.56	24.39	1.96	0.06	Beta
	Minimum Temperature	27.96	21.78	0.64	0.03	Normal
77.125/9.125	Precipitation	168.69	0	13.99	1.88	GEV
	Maximum Temperature	34.35	26.57	1.51	0.08	Gamma
	Minimum Temperature	27.26	21.56	0.09	0.03	Normal

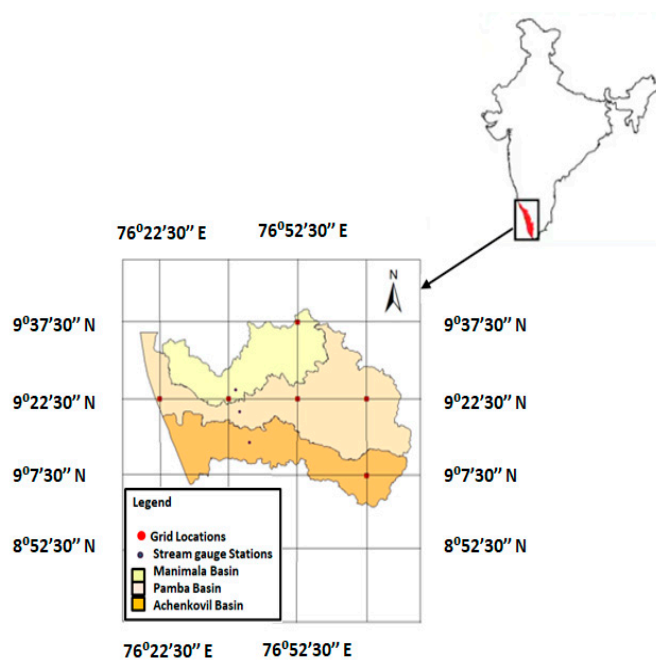


Figure 1. Location of stream gauge stations and contributory rainfall grid points in the Greater Pamba region, Kerala, India.

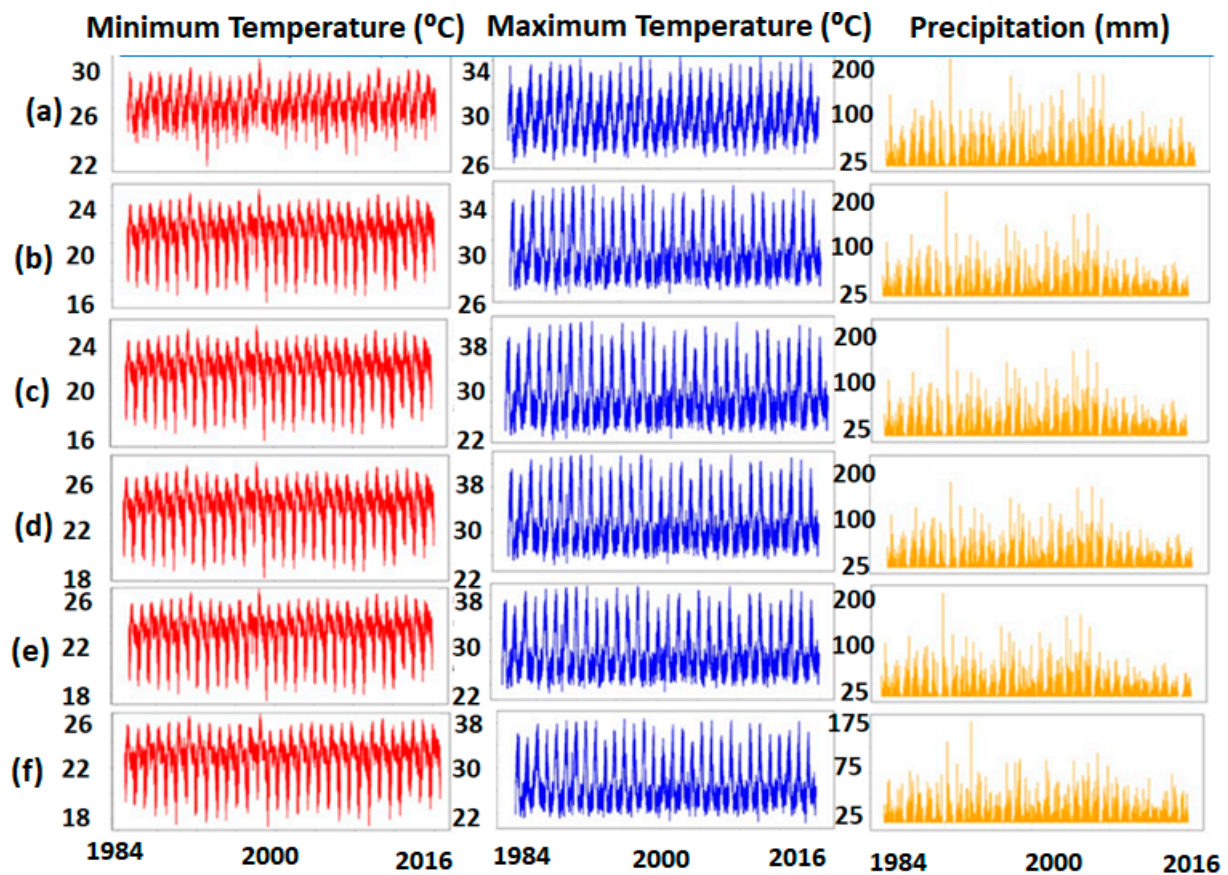


Figure 2. The time-series plots for daily precipitation and temperature obtained for the time period of 1985 to 2015 of the selected grid locations ((a–f) as shown in the Section 2.1) of GPRB.

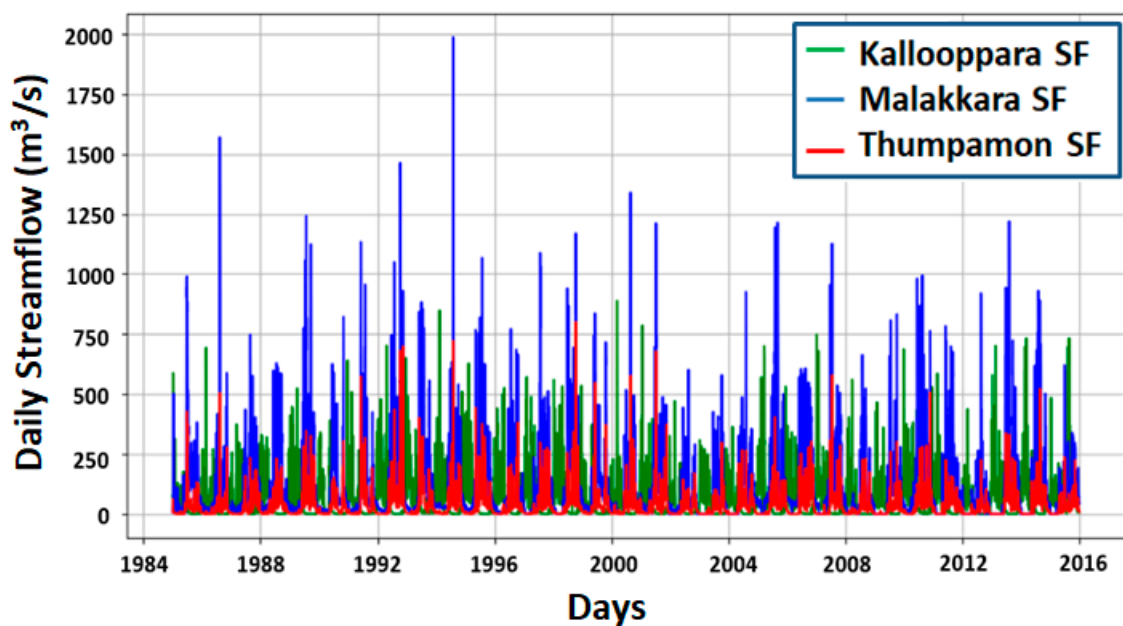


Figure 3. The time-series plots for streamflow (SF) measured at the selected stream-gauge stations of GPRB for the time period of 1985 to 2015.

2.2. Data Sources

The inputs used for the study includes the daily streamflow data for the three stream-gauge stations of GPRB–Thumpamon, Kallooppara and Malakkara, for a time period ranging from 1985 to 2015 (Obtained from Water Resources Information System–WRIS), bias-corrected climate projection GCM data (ACCESS-ESMI-5, INM-CM5-0 and MPI-ESMI-2-HR) for different scenarios of SSP126, SSP245 and SSP585, of CMIP6 [31], LULC data for the years of 1985, 1995, 2005 from Decadal LULC Classification and LULC for 2015 from BHUVAN platform of National Remote Sensing Centre (NRSC) with a resolution of 100 m and for carrying out the Reliability Ensemble Averaging (REA) corresponding precipitation and temperature daily data for the period of 1985 to 2015, are collected from India Meteorological Department (IMD) of 0.25×0.25 resolution and NASA Power respectively. The Digital Elevation Model (DEM) for the basin, with a horizontal resolution of around 30 m, is obtained from JAXA ALOS website. The REA is established using Bayesian Model Averaging and is carried out in Python platform. The LULC projections are determined in the GIS interface enabling the Cellular-Automata Markov Model and the final streamflow prediction in python platform using deep learning techniques of Long Short Term Memory model. All the public database links are provided in the Data Availability section.

2.3. Methodology

The overall methodology of the study follows the steps of Reliability Ensemble Averaging for multi-GCM ensembling, Cellular Automata (CA)-Markov Model for future LULC projection, overlaying of flow accumulation with LULC for drawing the influence of each land-use in streamflow pattern and the deep-learning technique of LSTM for future streamflow projections for different climate scenarios. The whole work-flow is as shown in Figure 4.

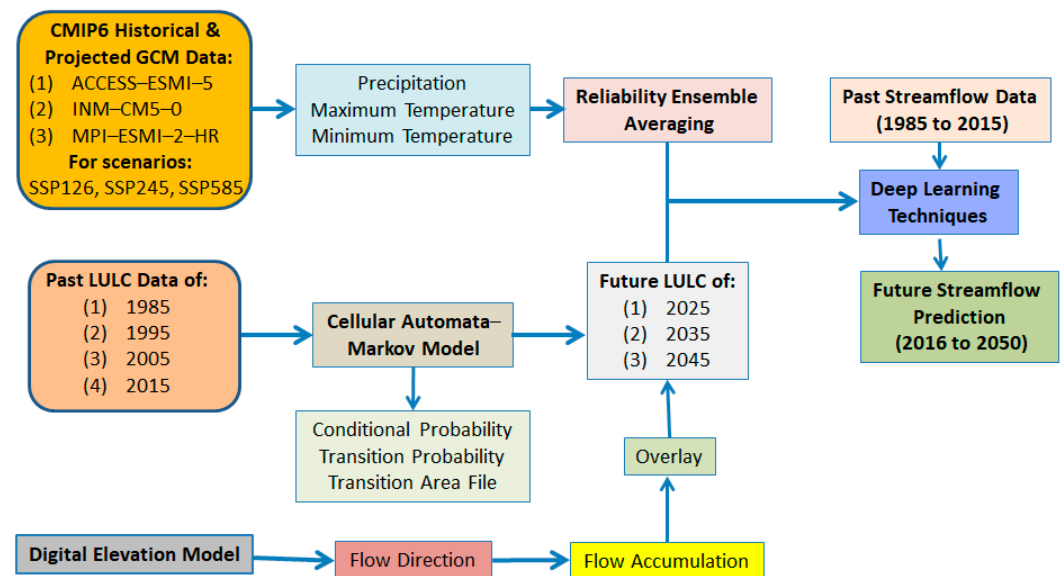


Figure 4. Overall work flow for basin-scale streamflow projection.

The primary data procured for the climate change analysis includes the climate projection GCM data (ACCESS-ESMI-5, INM-CM5-0 and MPI-ESMI-2-HR) for different scenarios of SSP126, SSP245 and SSP585, of CMIP6 [31]. GCM is a useful tool for generating future climate patterns, which is necessary to accurately understand the future effects of climate change on hydrological processes. If there are only slight biases between the simulated and observed data, bias correction is not necessary; otherwise, bias correction will be required while the model is inadequate for hydrological modelling. GCMs are often based on climatological hypotheses, which frequently lead to some non-ignorable errors when

compared to observable data. In order to reduce the mistakes of GCM outputs, the initial goal of bias correction is to make the GCM output as near to the relevant observed data as feasible [32]. The database developed by Mishra et al. [31] contains the bias-corrected precipitation, maximum temperature, and lowest temperature data for six South Asian countries. It comprises of 13 separate climate models, each of which include all the five scenarios listed as historical, SSP126, SSP245, SSP370, and SSP585. Reliability Ensemble Averaging (REA) is done for better accuracy. It is done to combine multiple bias corrected GCM projections with observed data to improve the reliability of climate change projections. In this study, for the analysis of REA of precipitation, historical India Meteorological Department (IMD) gridded data ($0.25^\circ \times 0.25^\circ$ spatial resolution) is considered and the reliability of each GCM is calculated by comparing its historical projections with the IMD observed data. This is done by how well each GCM's historical projections match the historical observations. The weights for each GCM are computed based on its reliability. In this study, the work is planned for the regional scale for whole basin. The climatic parameters, including the daily precipitation, maximum and minimum temperature, ranging from 1985 to 2015 for the 6 grid stations falling within the whole basin (2 in Manimala basin, 3 in Pamba and 1 in Achenkovil basin) and streamflow data from streamgauge stations of Kalliooppara, Malakkara and Thumpamon falling respectively in Manimala, Pamba and Achenkovil are considered for the regional-wise implementation of the framework. The streamflow in the rivers of Kerala, characterized by a tropical environment, is significantly influenced by precipitation. The monsoon season, which normally occurs from June to September, is defined by heightened precipitation, resulting in enhanced water input and elevated streamflow. The temperature, which remains relatively stable throughout the year due to the tropical climate, can influence the rates of evaporation and soil moisture, hence impacting the accessibility of water for streamflow in these rivers.

The anthropogenic influence on streamflow could be defined by the changing LULC of the basin. The spatial distribution of land cover classes, the estimation of hydrological parameters, the identification of land use changes affecting water resources, and the assessment of climate change impacts are all made possible by LULC data, which is of utmost significance in hydrological studies [33–36]. The reliability and efficiency of hydrological modelling are improved by using precise and current LULC data, which also helps with making suitable water management decisions. In this study, past LULCs of the study area with an interval of 10 years are considered, that is for 1985, 1995, 2005 and 2015. The projection of LULC (Land Use/Land Cover) data by CA-Markov Model, additionally proves crucial for hydrological research because it enables the evaluation of potential changes in land cover and their effects on hydrological processes. When examining the hydrological aspects that impact streamflow dynamics within a basin, it is crucial to emphasize the direct consequences of alterations in LULC on the processes of precipitation and runoff. The hydrological cycle may be greatly altered as a consequence of changes to LULC, which would then affect streamflow dynamics. The rate of penetration and water retention diminishes when natural vegetation is replaced by impermeable surfaces or urban development, which lowers groundwater recharge. The outcome is a rise in surface runoff and a fall in evapotranspiration, which together enhance the volume and speed of water entering streams. Due to these changes in hydrological pathways brought on by LULC alterations, streamflow is amplified, raising the danger of flash floods, erosive processes, and changed flow patterns in river systems. Thus, changes in LULC have the potential to cause rapid adjustments in the spatial patterns and intensity of precipitation losses. The alterations in plant cover, impervious surfaces, and other land features have a significant impact on the creation of streamflow, resulting in these losses playing a crucial part in changing the process. The inherent connection between land use and land cover changes and their impact on hydrological responses highlights the necessity of acquiring a thorough comprehension of how alterations in land cover might intricately affect the hydrological cycle.

The mere application of LULC patterns with the hydrological parameters are found to be less significant when compared with the combined effect of flow accumulation and

LULC. The benefit of employing flow accumulation layered on LULC for streamflow projection is that it can account for topographical features of the terrain and their impact on water flow. Hence, the hydrological interconnectedness and paths of water transport within a watershed can be better represented by integrating flow accumulation with LULC data, leading to more accurate streamflow estimates.

A comprehensive approach was employed for successfully integrating multiple geospatial datasets with different spatial resolutions and coverages. This technique involved the utilization of resampling and spatial aggregation methods. The LULC dataset, which has a spatial resolution of 100 m, was resampled by bilinear interpolation in order to align with the more detailed 30 m resolution of the Digital Elevation Model (DEM). Simultaneously, the precipitation data, which was originally provided at a resolution of $0.25^\circ \times 0.25^\circ$, was subjected to spatial aggregation. This involved LULC units into larger precipitation grid cells using a weighted mean method. These methods were implemented to guarantee that all datasets have similar spatial dimensions and alignments, hence facilitating meaningful comparison and analysis. The utilization of GIS software (ArcGIS version 10.3) facilitated the implementation of resampling and spatial aggregation procedures, which effectively ensured the compatibility of the data while also maintaining the integrity of the original information in each dataset. This process enhanced the dependability and precision of subsequent studies.

The final lap of the study explains the use of LSTM based deep learning environment for streamflow prediction. LSTM is found to be a sophisticated deep learning model that has gained favour in the prediction of streamflow [36–38]. LSTMs are a sort of recurrent neural network (RNN) that is used to solve the vanishing gradient problem and detect long-term relationships in sequential data. In the context of streamflow prediction, this model anticipates future streamflow using historical streamflow data as well as additional significant variables such as precipitation, temperature, and LULC values. Memory cells in the LSTM architecture retain and update information over time, allowing the model to learn complicated temporal patterns and represent the dynamics of hydrological processes. LSTMs can successfully understand the correlations between past and future streamflow observations by training on historical data, allowing for accurate and trustworthy streamflow forecasts.

2.3.1. Reliability Ensemble Averaging

REA is a potent method for multi-GCM ensemble that offers a reliable and precise method for climate forecast and prediction [39]. GCMs are mathematical simulations of the Earth's climate system that include a number of physical and chemical processes. Individual GCMs, however, frequently have inherent biases and uncertainties because of parameterizations and simplifications. In order to represent a variety of probable climatic scenarios, ensemble averaging integrates the outputs of many GCMs. Bayesian based REA is established in this study and is done for all the scenarios of SSP126, SSP245 and SSP585.

The fundamental premises of this approach are that the predictions have a symmetric distribution centred on the "true value", but with an individual variability to be viewed as a gauge of how well each model simulates the climate response to the specified collection of natural and human forcings. The weights for each model are allocated based on the skill score determined from Bayesian Model Averaging (BMA) (Equation (1)). The weights are proportional to the model's skill score in the Bayesian framework, indicates more precise and skilled models with larger weights. The degree of uncertainty surrounding each model's estimated using the true set of values. In this study, true values of precipitation are considered from IMD gridded data of 0.25×0.25 resolution and maximum and minimum temperature (for the grid point locations) from NASA Power. While meteorological station data are indeed valuable for their accuracy, and direct measurements, their use in comprehensive basin-scale studies can be hindered by two primary factors: data accessibility and spatial coverage. In many cases, meteorological station data might not be freely accessible or may be limited in spatial coverage, resulting in data gaps that can compromise the

accuracy of the analysis. In contrast, gridded datasets from organizations like the IMD offer a broader spatial coverage and availability, making them advantageous for large-scale studies. Given the constraints posed by data availability and coverage, we opted for the IMD's gridded dataset as it offered a reasonable compromise between data accuracy and coverage. It's important to note that these gridded datasets are derived from meteorological station data and various interpolation methods, aiming to provide a representation of true precipitation values across a larger spatial extent.

Both residual calibration errors and ambiguity in model parameters might contribute for the overall uncertainty. Combining the models, ensemble averaging is done (Equation (2)). Finally, the ensemble mean incorporates the advantages of each unique model to produce a more reliable estimate.

$$W(i) = \frac{\exp(Nss(i))}{\sum_{j=1}^n \exp(Nss(j))} \quad (1)$$

where $W(i)$ = Weight allotted for the models (i), Nss = Normalized skill score for each model i and j ranges from 1 to total number of models, here it is 3.

$$REAm = \sum_{i=1}^n (W(i) \times GCM(i)) \quad (2)$$

where $REAm$ = Ensemble mean for a selected variable, $GCM(i)$ = Values of GCM i .

2.3.2. LULC Projection by Cellular Automata (CA)–Markov Model

The CA-Markov Model is an effective technique for the simulation and projection of LULC [40–42]. To represent the spatiotemporal dynamics of LULC, it integrates ideas from cellular automata and Markov chain modelling. The research region is represented by a grid in the model, with each grid cell corresponding to a land unit. The CA-Markov Model creates a transition probability matrix using previous LULC data that measures the likelihood to switch from one LULC class to another [43]. LULC distribution and change are governed by spatial transition criteria based on terrain, accessibility, and the composition of the nearby land cover. By randomly assigning new land cover classes to grid cells in accordance with the transition probabilities and spatial rules, the model simulates LULC changes over time. With its ability to explore prospective LULC dynamics, this framework helps with land management, planning, and environmental assessments by illuminating potential patterns and trends of land use and land cover in space [41].

In this study, CA-Markov model is established using Methods of Land-Use Change Evaluation (MOLUSCE) plugin in QGIS 2.18 software. This plugin is extensively used to forecast future LULCs [44–47]. It trains input data using the Multilayer Perceptron-Artificial Neural Network (MLP-ANN). This integrated framework utilizes the CA model to simulate the spatial dynamics of LULC changes by considering the local interactions and transitions between different land cover categories, while the Markov process incorporates historical transition probabilities to capture the temporal trends in LULC alterations. This combined approach, facilitated by the MOLUSCE plugin within QGIS, enables the generation of predictive scenarios for future LULC patterns, providing valuable insights into potential landscape transformations. For this study, the LULC variations are considered for predicting the future streamflow of the selected basin. Accordingly, we have collected the LULC maps at decadal intervals for the years of 1985, 1995, 2005 and 2015 from the sources like decadal LULC classification and Bhuvan platform of NRSC. The study tends to establish the usage of future LULC in streamflow forecasting. Therefore, the future predictions of LULC are carried out using this CA-Markov model. Thus, the LULC projections for the decadal intervals of 2025, 2035 and 2045 are employed. The projections for all these years are determined using the available LULCs of 2005 and 2015. Basically, there are two different approaches for LULC projection. They are: Single step and Multi-step approach. In the former approach, the LULC maps from 2005 and 2015 are used as inputs to the CA-Markov model to project the LULC for 2025, 2035, and 2045 independently. The model

would use the historical transition probabilities derived from the 2005–2015 period to simulate the changes for each projection year. This approach assumes that the relationships between land cover changes observed in the 2005–2015 period remain consistent for future years. In the latter approach, the LULC maps from 2005 and 2015 are used to project the LULC for 2025. Then, for projecting 2035, the 2015 map along with the projected 2025 map are used. Similarly, for 2045, using the 2025 and 2035 maps. This approach takes into account the progressive changes over time and allows for adjustments based on the changing conditions observed in earlier projections. The single-step approach is simpler and assumes a consistent relationship between the reference years and future years. The multi-step approach accounts for potential changes in relationships over time but can also introduce compounding uncertainties due to the cascading nature of projections. Therefore, considering the avoidance of uncertainties, single step approach is applied here.

The input data consists mostly of pixels from initial state rasters and factor rasters. After receiving the inputs, the model performs initial data pre-processing (dummy coding and normalisation), sampling, and training. MOLUSCE employs a multilayer perceptron together with the numpy tanh sigmoid function. As a result, during dummy coding, target variables (the change map categories) should be scaled to the $(-1, 1)$ interval rather than the $(0, 1)$. The number of hidden layers and neurons (one or more) may be adjusted at the user's choice. The network's number of input neurons is provided by:

$$\{(Cn - 1)(2Ns + 1)(2Ns + 1)\} + \{(2Ns + 1)(2Ns + 1)\} \quad (3)$$

where Cn is the number of land use categories and Ns is the user-specified neighbourhood cell size. The classic back propagation approach with momentum is used in the module's learning process. The corrections on weights are to be done as follows:

$$(j + 1) = Lr \times j + m \times (j - 1) \quad (4)$$

where j is the number of iterations, Lr represents the learning rate, and m is generally a count of distinct categories in the change map and is the same as the number of output neurons in the generated network (momentum), which depends on the sampling mode.

The module delivers the errors (mean of all errors on the learning and validation sets) calculated on each set after every phase. The achieved weights are saved, and the best weights are preserved and updated afterwards. On the validation set, Delta overall accuracy (difference between minimum validation error and current validation error) and Current validation kappa are eventually accomplished [47].

The Figure 5 shows the LULC inputs from 1985 to 2015 at ten year interval for the future projection. The LULC map study reveals the various land-cover classes within the study area. In consideration of the specific objectives of this study, which involve the future prediction of streamflow patterns using LULC and climate data, we focused the analysis on the major land use classifications that significantly impact streamflow dynamics. Thus, reclassification on LULC dataset is done based on hydrological criteria by consolidating several classes into broader categories such as Water body, forest, grassland, agriculture, built-up, shrub, bare ground and others. The forest occupies the largest area within this basin. The rationale behind this reclassification lies in the intention to capture the most influential LULC classes that directly influence streamflow. By focusing on these significant categories, we aim to streamline the analysis process and enhance the clarity of the findings. These prominent land use classifications are expected to have a pronounced impact on hydrological behavior, aligning with the scope of this research.

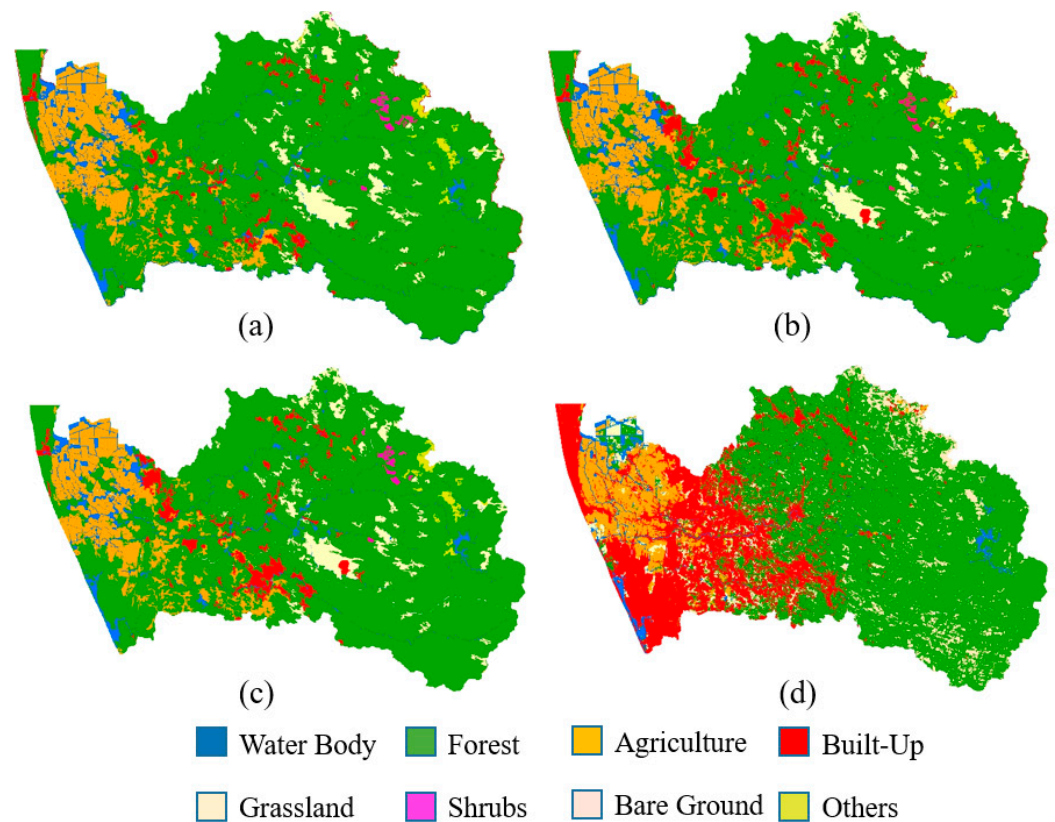


Figure 5. Land-Use Land Cover maps of GPRB for the years (a) 1985 (b) 1995 (c) 2005 and (d) 2015.

2.3.3. Flow Accumulation–LULC (FA-LULC) Overlay

Flow Accumulation is a key notion in hydrological modelling that measures the accumulation of water as it moves downstream [12]. It is calculated by analysing a Digital Elevation Model (DEM) and computing the cumulative input from upstream cells. FA gives insights into drainage patterns, aids in the delineation of stream networks, and is critical in calculating streamflow and other hydrological parameters. Its use in hydrological modelling helps to improve knowledge of water movement and facilitates numerous research connected to water resource management and analysis.

Obtaining flow accumulation in hydrological modelling entails multiple phases. The DEM gives information on the terrain's levels across the landscape. Various techniques may be used to detect the direction of flow at each cell or pixel using the DEM. This entails determining the steepest descending path or flow direction between each cell and its neighbouring cells. After determining the flow direction, the cumulative flow at each cell is calculated. This is accomplished by adding the intake from all upstream cells. Starting at the basin's edge, the accumulated flow is carried downstream, increasing as water from surrounding cells flows into it. This process is repeated until the whole basin has been covered, and flow accumulation values are assigned to each cell.

In the context of hydrological model-based investigations, the combination of FA-LULC is significant [48]. Streamflow prediction models can better describe the geographical distribution of water movement and flow channels within a watershed by integrating LULC data with flow accumulation. FA takes topography features and drainage patterns into consideration, whereas LULC data gives information on land cover types and their qualities. By combining these two datasets, we can get a more precise picture of how land cover changes affect water flow and streamflow generation.

The procedure of overlaying LULC and FA data requires the same level of spatial resolution. Various approaches, such as ArcGIS's Zonal Statistics tool, can be used to overlay the FA-LULC grid. This tool computes statistical summaries for each zone defined by the flow accumulation cells, such as the mean, maximum, or majority land cover type.

The LULC properties are connected with the corresponding flow accumulation cells using the Zonal Statistics tool. This gives useful information on the mix of land cover within each zone of accumulated flow.

The correlation between land cover types and cumulative flow must next be investigated. This analysis may include assessing the impact of various land cover classes on streamflow generation, identifying areas of interest or hotspots where specific land cover changes have a significant impact on streamflow patterns, and investigating the spatial distribution of land cover types in the context of flow accumulation. The aggregated land cover characteristics within each flow accumulation zone are supplied to the model by using statistical summaries from the zonal table as inputs into the prediction model. This can assist the model in capturing the impacts of land cover fluctuations on streamflow patterns and improving streamflow forecast accuracy.

The DEM and flow accumulation maps considered for the study are as shown in the Figure 6. The zonal statistics summary is to be determined in regional scale for all the selected years of suitable intervals.

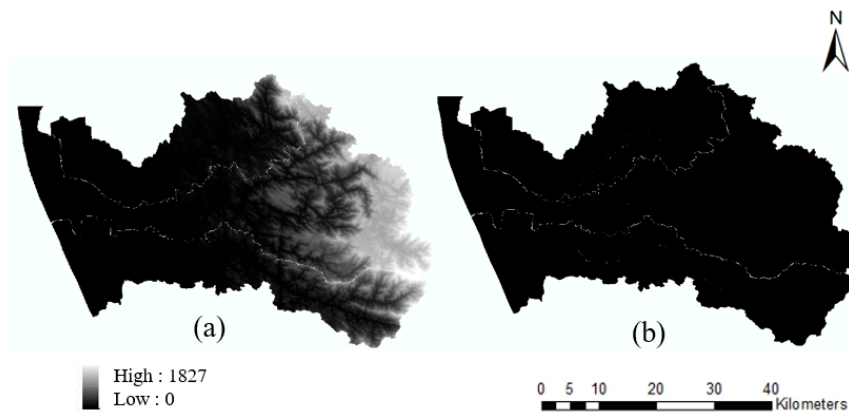


Figure 6. (a) Digital Elevation Model and (b) Flow Accumulation of GPRB with basin-wise demarcations.

2.3.4. LSTM for Future Streamflow Projection

Due to their proficiency with sequential data, recurrent neural networks (RNNs) are a robust family of deep learning models frequently utilized for streamflow prediction [49,50]. For applications like estimating streamflow, RNNs are very effective at identifying temporal connections and patterns in time series data. It's crucial that the effectiveness of the RNN model for streamflow prediction depends on a variety of elements, including the quality and quantity of the input data, model design, hyper-parameter tuning, and the intrinsic complexity of the streamflow dynamics.

LSTMs, a subclass of RNN, are ideally suited for modelling and forecasting streamflow patterns since they were created with the goal of capturing long-term relationships in time series data [35]. For such prediction challenges, these networks have significant benefits over standard RNN. By combining memory cells and gates that selectively preserve and update information over extended time intervals, LSTMs overcome the vanishing gradient problem typically observed in RNNs [38]. This allows LSTMs to detect long-term relationships in streamflow data, which is critical for effective prediction. Furthermore, LSTMs excel at dealing with time-lag patterns, modelling links between previous streamflow measurements and future forecasts. They can handle variable-length sequences, which is important for datasets that have anomalies or missing data. The memory and forget gates of LSTMs allow for selective knowledge retention and discarding, allowing focused learning. Furthermore, they prevent gradient vanishing and explosion during training, resulting in more stable and efficient model optimization [38]. Overall, LSTM networks outperform other networks in terms of capturing long-term dependencies, dealing with time-lag patterns, supporting variable-length sequences, and resolving gradient-related issues, making them a favored choice for streamflow prediction in hydrological investiga-

tions [36]. The hyper-parameters and composition of LSTM layer considered for this work is given in Table 2.

Table 2. The hyper-parameters and composition of LSTM layer considered for this work.

Model	Activation Function	Hidden Layer 1	Dropout	Hidden Layer 2	Dropout	Hidden Layer 3	Dense Layer 1	Dense Layer 2
LSTM	ReLU	LSTM 75 Units	0.25	50 Units	0.5	50 Units	25 Units	1 Unit

Following the aforementioned methodology, the streamflow projection for three different scenarios of SSP126, SSP245 and SSP585 ranged up to 2050 for all the three stations in the GPRB is carried out. The prediction is done in two steps: One considering only the climate variables and the other, considering the FA-LULC parameters along with the climatic inputs for comparing the prediction accuracies.

3. Results

3.1. Reliability Ensemble Averaging for Multi-GCM Simulations

The bias-corrected climatic data, for six grid points falling over the basin, from the GCMs of ACCESS-ESMI-5, INM-CM5-0 and MPI-ESMI-2-HR [31] are selected for this study. The whole basin is considered on a regional scale for the entire work, with the basins of Manimala, Pamba and Achenkovil as individual entities. The model parameters for each of the GCMs are combined by means of REA method and the resulted new set of parameters are passed on to the streamflow prediction technique. The Figure 7 represents the monthly REA mean (for the parameters of precipitation, maximum and minimum temperature) of the selected grid points of Pamba for the extreme (SSP585) scenario.

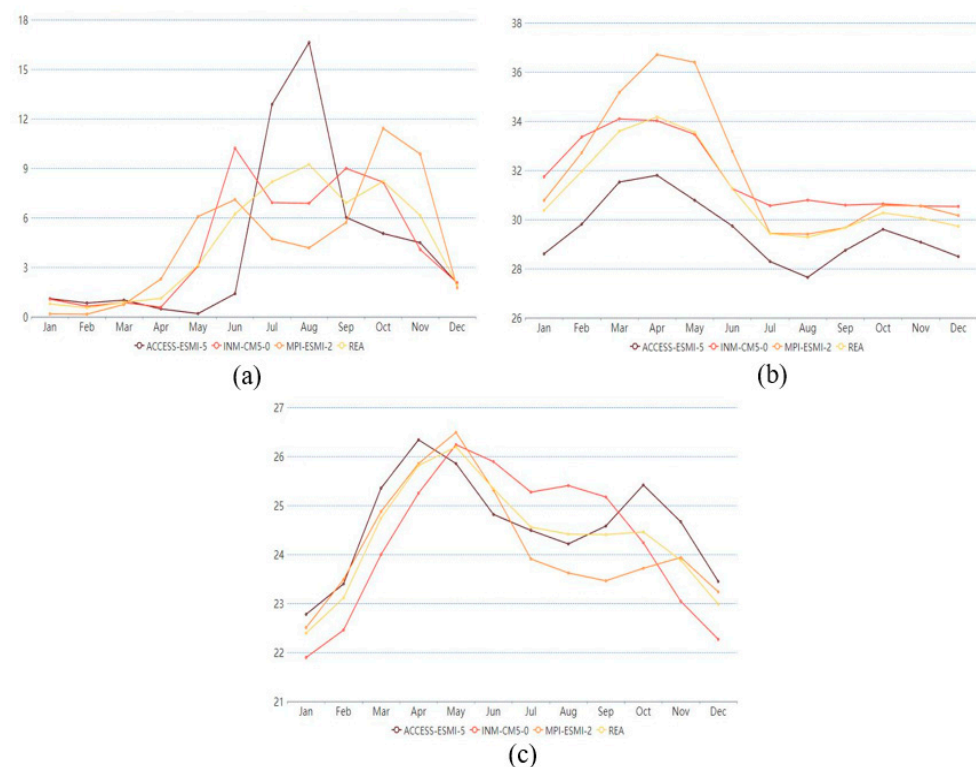


Figure 7. Monthly mean REA of (a) Precipitation (mm) (b) Maximum Temperature (°C) (c) Minimum Temperature (°C) for selected station points of Pamba.

3.2. Future LULC Projection Using CA-Markov Model–MOLUSCE Plugin

The future LULC maps from 2025 to 2045 at ten-year intervals were simulated using the historical LULC maps (1985 to 2015) of the GPRB, and the resulting LULC maps are displayed in Figure 8.

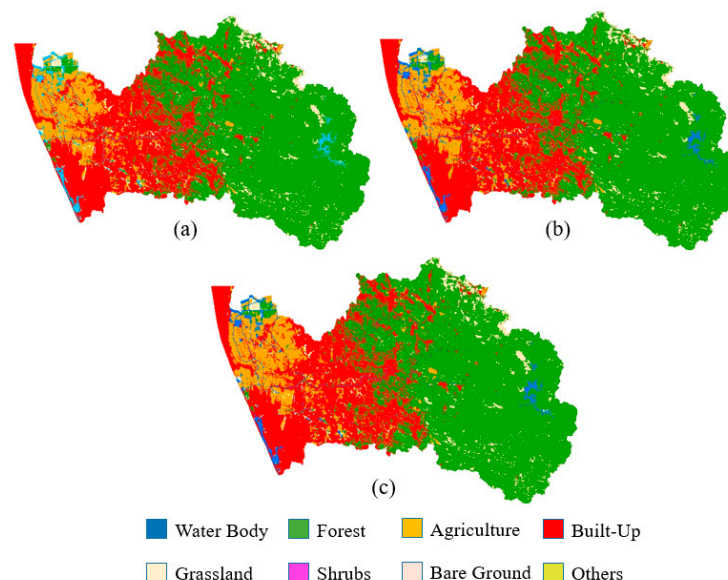


Figure 8. Land-Use Land Cover maps of GPRB from CA-Markov model for the years (a) 2025 (b) 2035 (c) 2045.

From 2025 to 2045, there is a substantial growth in the built-up area, as seen in Figure 6. Figure 9 presents a visual representation of the percentage area changes for historical (1985), base (2015) and future period (2045) of GPRB. This plot shows that between 1985 and 2045, there will be a clear decline in the amount of forested land and a sharp rise in the amount of built-up land. Rapid urbanization, population increase, and economic expansion may be at blame for this. The forest area declined to 2568.02 km² from 3660.62 km². The total area under construction has grown from 79.89 km² to 1252.97 km², while the total area under cultivation has grown from 261.13 km² to 399 km². The other five land use classifications similarly exhibits varying tendency, but with a smaller amplitude.

A validation analysis carried out for the LULC of a selected year of 2020 is as shown below. It is done by overlaying the actual and predicted LULCs in ArcGIS. The actual LULC is obtained from ESRI LULC dataset accessed on 2 February 2023 (<https://livingatlas.arcgis.com/landcover/>). It is then compared with the LULC of 2020 projected using the LULCs of 2005 and 2015 by means of CA-Markov model and the obtained confusion matrix is as shown below (Table 3). The considered land use classes are water body, forest, grassland, agriculture, built-up, shrub, bare ground and others.

The accuracy determination is done using various parameters and they are obtained as follows:

1. Overall Accuracy = (Sum of correctly classified pixels/Total no: of pixels) = 0.995
2. Producer's Accuracy = (User's accuracy for actual class 'Water Body') = 0.968
3. Precision = True Positive/(True Positive + False Positive) for 'Water Body' = 0.98
4. Recall = True Positive/(True Positive + False Negative) for 'Water Body' = 0.968
5. F1 Score = 2 × (Precision × Recall)/(Precision + Recall) for 'Water Body' = 0.974

All these values manifested the accuracy of LULC projection using CA-Markov model.

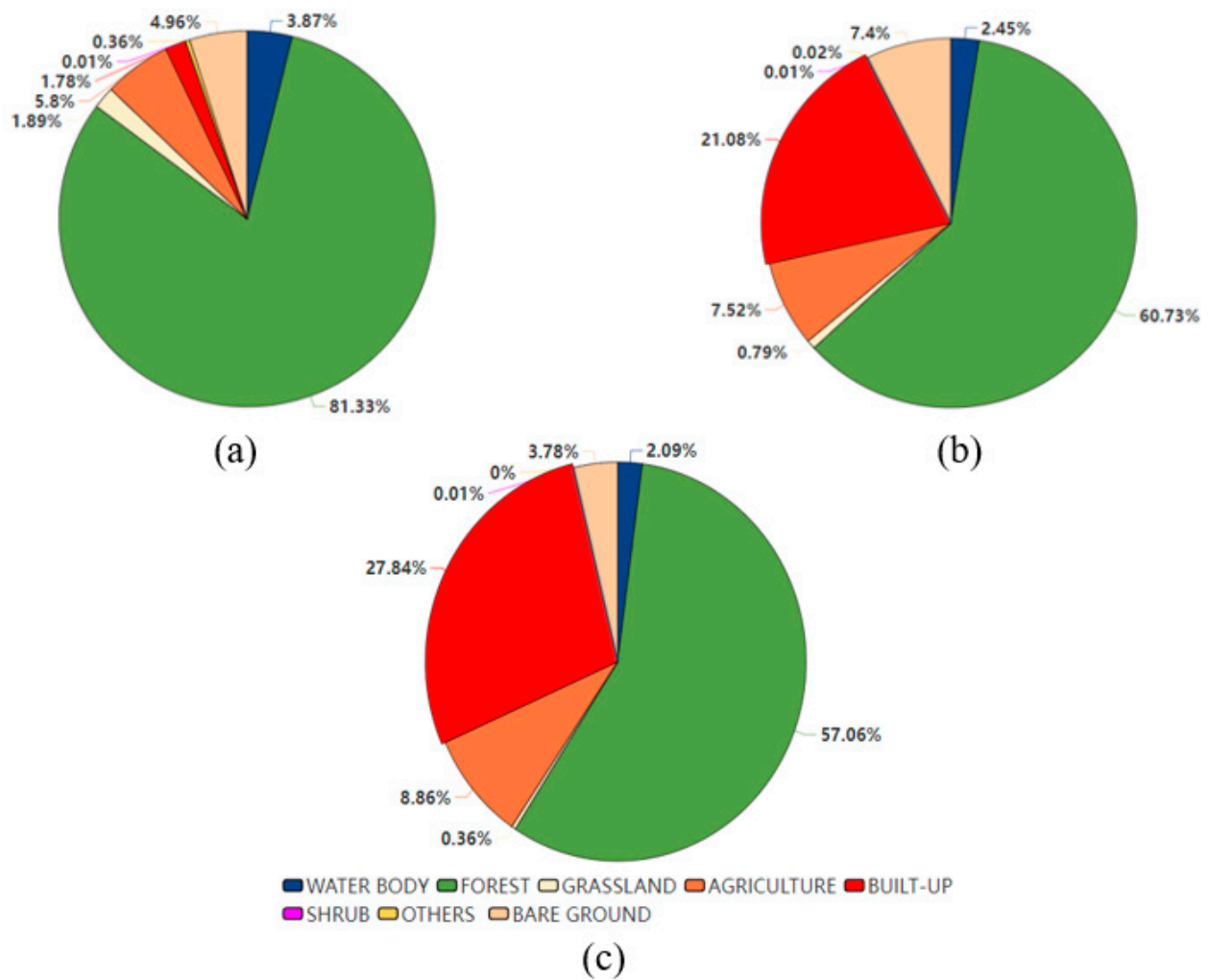


Figure 9. Pie-Chart for the percentage area changes for (a) historical (1985), (b) base (2015) and (c) future period (2045) of GPRB.

Table 3. Confusion matrix showing LULC Validation using actual and predicted land use classes for the year 2020.

Actual Classes	Water Body	Forest	Grassland	Agriculture	Built-Up	Shrub	Bare Ground	Others
Predicted Water body	1,013,222	12,368	758	876	18,888	78	0	101
Predicted Forest	7541	25,510,333	2563	958	16,523	196	0	189
Predicted Grassland	251	15,651	115,231	772	13,269	101	0	336
Predicted Agriculture	4470	14,789	3589	4,100,777	17,536	111	0	2358
Predicted Built-Up	2517	1369	523	638	11,548,354	0	0	63
Predicted Shrub	1888	7569	999	1056	19,638	4012	0	785
Predicted Bare Ground	986	14,500	478	987	11,258	53	2	569
Predicted Others	2288	5431	5270	3712	9175	110	0	2,490,030
Total	1,033,163	25,582,010	129,411	4,109,776	11,654,641	4661	2	2,494,431

3.3. Flow Accumulation-LULC Overlay Using Zonal Statistics

The purpose of this study was to investigate the relationship between flood accumulation and the geographical distribution of LULC categories in a given area. By superimposing these two datasets and utilizing ‘zonal statistics as a table’ in ArcGIS, useful insights into the spatial patterns and possible repercussions of flood episodes on different land cover categories were achieved.

The resulting table from the zonal statistics analysis comprised an array of statistical measures, including the total area of each land cover type impacted by floods, the average flood accumulation value within each category, and the maximum and minimum flood accumulation values. These figures enabled a comprehensive assessment of the impact of floods across various land cover types. The statistics summary was calculated for the years 1985, 1995, 2005, 2015, 2025, 2035, and 2045 (for which LULC was considered). The Table 4 below summarizes the FA-LULC statistics of Pamba for the base year of 2015.

Table 4. FA-LULC overlay statistics of Pamba Basin for the base year of 2015.

Value	Label	Count	Area (km ²)	Min	Max	Range	Sum
1	Water Body	298,526	29.8526	1	9	8	315,895
2	Forest	9,001,197	900.1197	1	9	8	9,040,508
3	Grassland	40,065	4.0065	1	3	2	40,238
4	Agriculture	1,183,885	118.3885	1	9	8	1,185,904
5	Built-Up	1,845,417	184.5417	1	9	8	1,855,177
6	Shrub	1584	0.1584	1	8	7	1640
7	Others	4517	0.4517	1	2	1	4518
8	Bare Ground	937,272	93.7272	1	7	6	939,986

There are several variables that might affect the overall flow accumulation. The total area of each land cover type is one of them. A larger area for a land cover class often indicates that there is more surface area available to contribute flow. In the table above, the forest is having highest area and is significantly contributing to the flow accumulation. FA is also estimated by analyzing the watershed’s flow paths and topographic features. For every location, it indicates the total upstream contributing area. FA patterns are significantly influenced by a number of other variables, including soil parameters, land cover characteristics, and hydrological processes. These elements may have an impact on how water moves and is retained within various land cover classifications, which may have an impact on flow accumulation values.

The “sum” column from the output of the zonal statistics denotes the sum or accumulation of the flow within each zone (in this example, the LULC classes). Therefore, it would be the ideal approach to illustrate how much each LULC class weighs in this scenario. The relative contribution of each LULC class to the flow accumulation is expressed by allocating weights to the LULC classes based on this. For a given LULC class, the higher the value in the “sum” column, the more that class contributed to the flow accumulation in that zone. The Min and Max columns reflect the lowest and highest FA values observed for each kind of land cover. Within each land cover class, it shows the distribution or variability of flow accumulation. Once the weights have been assigned, the analysis that follows can employ this information to account for the impact of flow accumulation on the weighted LULC classes.

Furthermore, the zonal statistics analysis indicated the geographical distribution of flood-affected land cover categories. For example, it was discovered that agricultural areas near rivers or low-lying areas were greatly influenced by flooding, potentially resulting to agricultural losses and disruptions in food supply. These findings give substantial insight into the association between flood episodes and LULC trends. They may contribute

to better understanding of flood risk management, urban planning, and land use policy as well. It is equally vital to recognize that the precipitation plays a crucial role in the occurrence of flood events. However, it is worth noting that the interaction between LULC modifications and precipitation patterns can have a substantial impact on the magnitude and intensity of floods. In flood dynamics, the intensity and amount of precipitation are pivotal factors that can trigger and amplify flood events. Torrential rain, characterized by its high intensity and short duration, can lead to rapid and excessive runoff, overwhelming drainage systems and natural watercourses. Such singular and intense precipitation events, rather than the average accumulation over a given period, often serve as the primary catalysts for flash floods and severe inundations. Recognizing the critical role of these acute precipitation episodes is essential for accurate flood forecasting, timely emergency response, and the development of resilient flood management strategies. Effective flood risk mitigation necessitates a comprehensive understanding of the interplay between precipitation patterns, land characteristics, and hydrological pathways, enabling proactive measures that account for both individual extreme events and long-term hydrological trends. The accuracy of capturing flood peaks through precipitation data and land use depends on various factors. The accuracy of precipitation forecasts can be impacted by the data's spatial and temporal resolution, as well as the availability of real-time observations. Land use also has a profound effect on flood risk since urbanization and changes in land cover can have an influence on runoff patterns, either escalating or reducing flood hazards. Therefore, to accurately capture flood peaks, it's essential to have high-quality precipitation data and consider land use changes and their impact on local hydrology. Floods commonly arise from singular, intense occurrences characterized by heavy rainfall. Accordingly, the interplay between precipitation and the geographical features of a region can significantly impact its susceptibility and capacity to withstand flooding.

3.4. Regional-Wise Future Streamflow Projection Using LSTM

This section analyses the effectiveness of LSTM model for future streamflow projection. The streamflow projection is carried out for two phases—with and without FA-LULC overlaid parameters. The climatic variables are considered on both the cases. The model efficiencies are measured using various error metrics like R-Squared (R^2), Root Mean Square Error (RMSE), Mean Absolute Error (MAE), Mean Square Error (MSE) and Nash-Sutcliffe Efficiency (NSE). The overall result analysis establishes the LSTM model with both the inputs of FA-LULC and climatic parameters as the superior one, which outperforms the LSTM model with climate variables alone as the input. The streamflow projection for all three SSPs obtained from LSTM for climate only and FA-LULC-Climature integrated phases are as shown in the Figure 10. The performance measures for each SSPs for both the phases are given in the Table 5.

R^2 is a statistical measure that demonstrates the extent to which the independent variables (features) of the model can explain the variation in the goal (dependent variable). A perfect fit is indicated by an R^2 value of 1, whereas a value of 0 indicates that the model is unable to account for any variance in the target variable. For Kalloppaara station, the R^2 for first phase (input function = FA-LULC and Climate) and the second phase (input function = Climate only) are obtained as 0.9 and 0.87 (for SSP126), 0.92 and 0.89 (for SSP245) and 0.91 and 0.88 (for SSP585) respectively.

Another kind of model evaluator is Root Mean Square Error (RMSE), which offers a measure of the overall model error, with a lower RMSE indicating better model performance. It is especially effective when errors are typically distributed and the data contains no outliers. Considering the Kalloppaara station, the RMSE for first phase and the second phase are obtained as 27.24 and 31.89 (for SSP126), 26.31 and 27.47 (for SSP245) and 26.62 and 29.08 (for SSP585) respectively.

Table 5. Performance measures for all SSPs for the Climate + LULC and LULC only phases.

Performance Evaluators	R ²	RMSE	MSE	MAE	NSE
KALLOOPPARA SSP126					
Climate + LULC	0.9	27.24	742.11	10.07	0.91
Climate	0.87	31.89	1017.17	13.12	0.86
KALLOOPPARA SSP245					
Climate + LULC	0.92	26.31	692.25	7.63	0.92
Climate	0.89	27.47	754.95	8.79	0.9
KALLOOPPARA SSP585					
Climate + LULC	0.91	26.62	708.71	9.16	0.92
Climate	0.88	29.08	846.15	12.09	0.89
MALAKKARA SSP126					
Climate + LULC	0.99	13.58	184.68	8.07	0.97
Climate	0.95	21.33	454.97	12.68	0.99
MALAKKARA SSP245					
Climate + LULC	0.99	5.12	26.17	3.04	0.97
Climate	0.95	10.37	107.49	6.16	0.94
MALAKKARA SSP585					
Climate + LULC	0.98	17.97	323.02	10.68	0.97
Climate	0.94	33.01	1089.09	19.62	0.95
THUMPAMON SSP126					
Climate + LULC	0.97	10.97	120.36	5.61	0.96
Climate	0.92	13.94	194.37	7.13	0.9
THUMPAMON SSP245					
Climate + LULC	0.99	1.76	3.11	0.91	0.98
Climate	0.91	4.68	21.98	2.34	0.91
THUMPAMON SSP585					
Climate + LULC	0.99	3.58	12.79	1.83	0.98
Climate	0.97	6.21	38.45	3.17	0.96

The Mean Absolute Error (MAE) equation is used to calculate the average absolute difference between the target variable's predicted and actual values. It represents the average size of the forecast's inaccuracies, regardless of their direction. For the Kallooppa station, the MAE for the first and second phases are 10.07 and 13.12 for SSP126, 7.63 and 8.79 for SSP245, and 9.16 and 12.09 for SSP585. MSE is a measure of the average squared difference between the predicted and actual values of a target variable. It is susceptible to outliers because it prefers larger mistakes over smaller ones. Considering the Kallooppa station, the MSE for the first and second phases are 742.11 and 1017.17 for SSP126, 692.25 and 754.95 for SSP245, and 708.71 and 846.15 for SSP585.

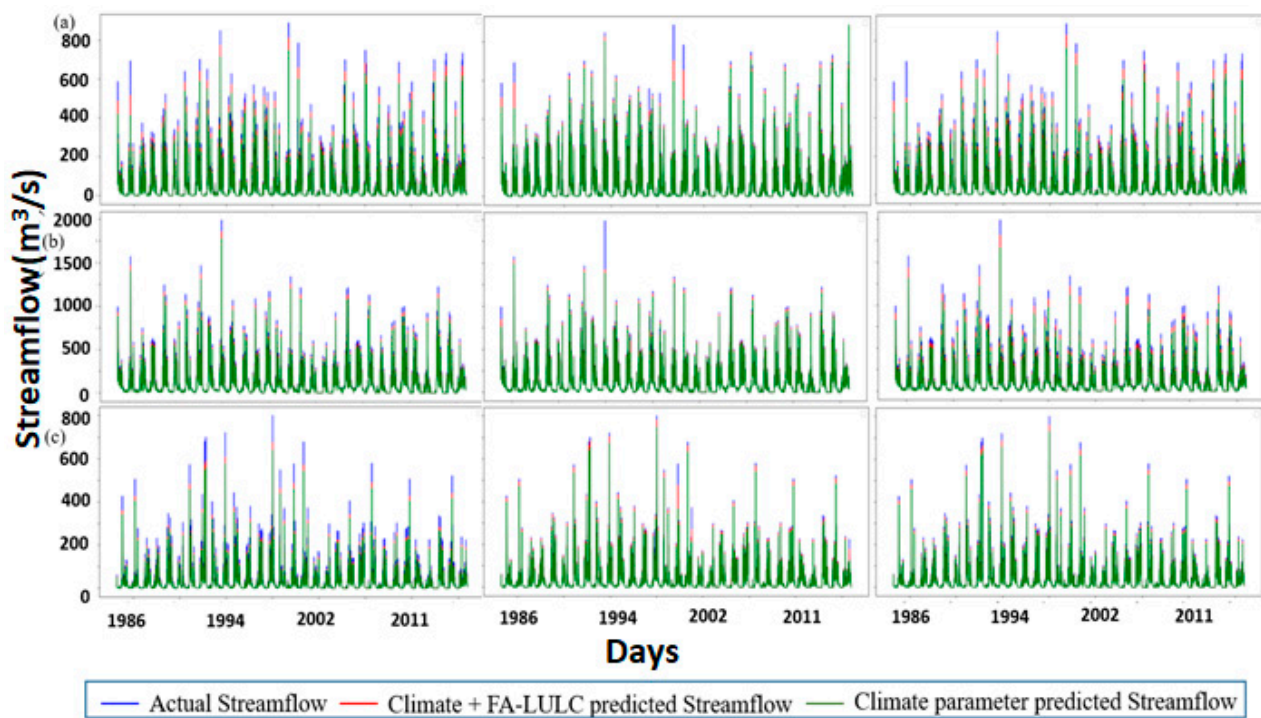


Figure 10. LSTM streamflow projection for all three SSPs (SSP126, SSP245, and SSP585) by Climate only and FA-LULC-Climate integrated phases for (a) Kallooppa (b) Malakkara (c) Thumpamon.

The Nash Sutcliffe Efficiency (NSE) of a model is a measure of how effectively it predicts outcomes. It compares the variance of the predicted values to the variance of the actual values, with a value of 1 indicating excellent predictions and values less than 0 indicating poor forecasts. The NSE for the first and second phases of the Kallooppa station are 0.91 and 0.86 for SSP126, 0.92 and 0.9 for SSP245, and 0.92 and 0.89 for SSP585. The performance evaluation is done graphically by plotting the scatter diagrams for all the SSPs (for the historical streamflow values from 1985 to 2015) and is given in Figure 11.

Additionally, by utilizing statistical measurements like mean and standard deviation, we specifically concentrated on identifying extreme streamflow values and is classified as high and low extremes by establishing criteria based on these measurements ($\text{mean} \pm (2 \times \text{standard deviation})$). This analysis is carried out for both the climate-FA-LULC induced projection and climate only induced projection. Extreme streamflow events have the potential to have a big influence on environmental planning, flood risk assessments, and water resource management. The high and low extremes analysis of Kallooppa for the extreme scenario of SSP585 are as shown in the Figure 12 as a general representation. The analysis establishes the significance of incorporating the FA overlaid-weighted LULC along with the climatic factors for streamflow projections under extreme conditions. For Kallooppa (with SSP585 scenario), R^2 for climate-FA-LULC induced projection is 0.8155 and 0.9125 for high and low extremes.

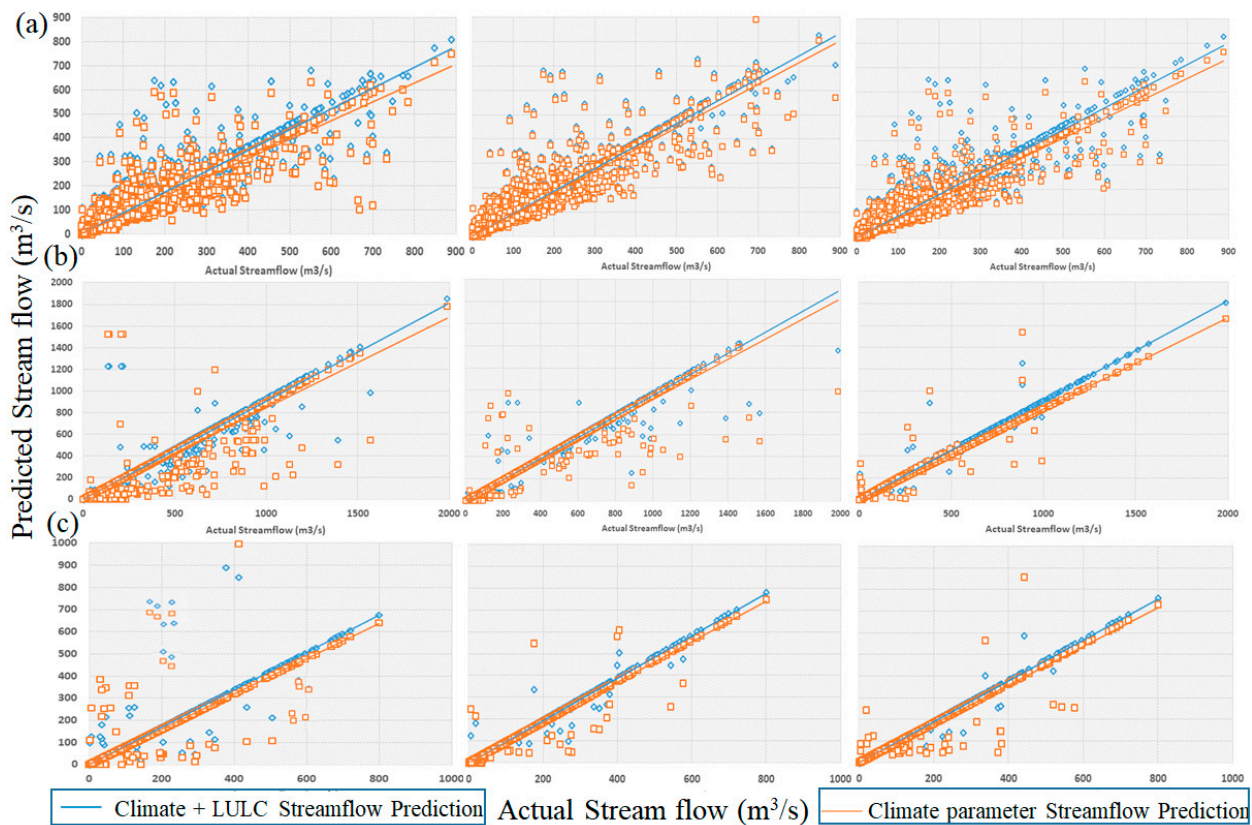


Figure 11. Scatter Diagrams for the scenarios SSP126, SSP245, and SSP585 of (a) Kallooppara (b) Malakkara (c) Thumpamon considering the cases of climate + LULC parameters and climate only parameter prediction.

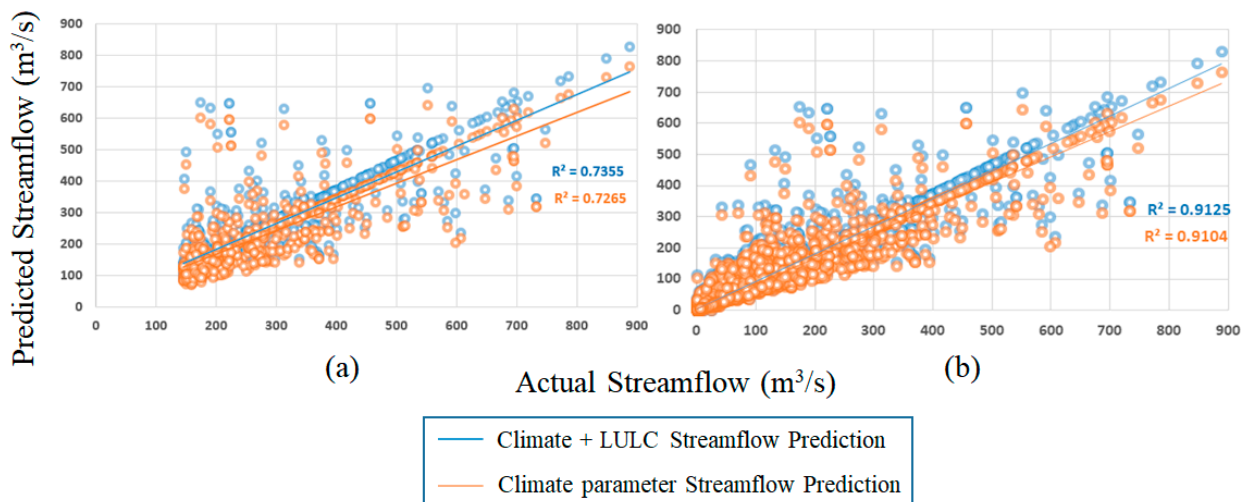


Figure 12. Scatter Diagrams for the (a) High and (b) Low extreme streamflow values of Kallooppara for extreme scenario condition (SSP585) considering the cases of climate + LULC parameters and climate only parameter prediction.

The past and predicted annual average streamflow for all the scenarios are plotted in Figure 13 for better understanding. The graph depicts the changes in streamflow patterns through time as well as prospective future scenarios. The blue line, which represents the observed past streamflow, serves as a reference for comparing anticipated streamflow under various SSPs. It displays historical streamflow patterns, which allows for a better

knowledge of baseline circumstances. The estimated streamflow curves for the various SSPs show the possible effects of various socioeconomic development routes on streamflow. The colour variation (red, green, and yellow) corresponds to the range of streamflow predictions associated with each SSP. The discrepancies in the graphs show how sensitive streamflow is to various socioeconomic and climate change scenarios. The Mann-Kendall test showed a monotonically increasing trend for all the SSPs, of the three stations considered, at a significance level of 5%. Considering Malakkara station, the historical data from 1985 to 2015 shows a decreasing trend with the SSP projections having increasing trends.

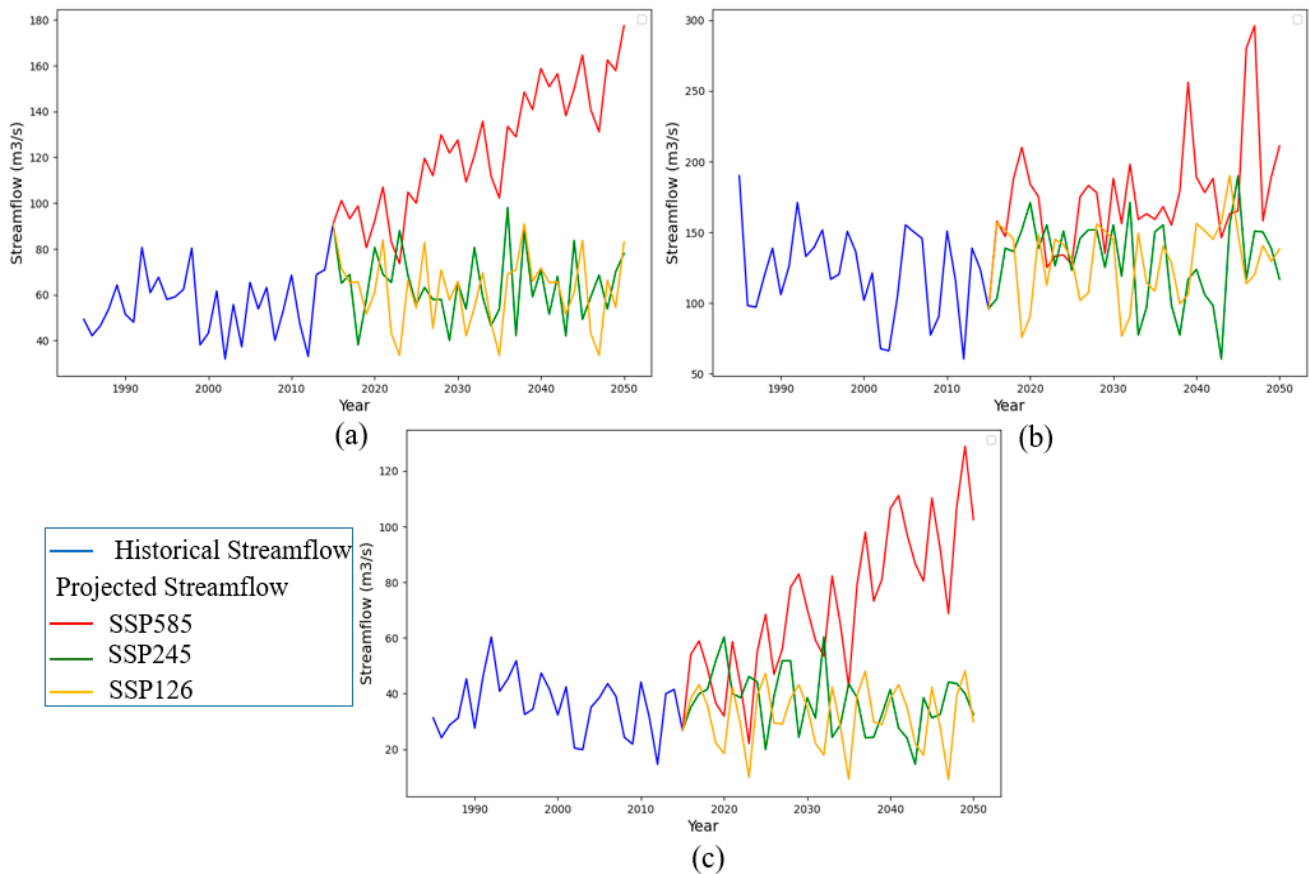


Figure 13. Historical and projected annual average streamflow from 1985–2050 for the scenarios SSP126, SSP245, and SSP585 of (a) Kalloopara (b) Malakkara (c) Thumpamon.

This graph is a useful tool for discussing projected streamflow variations in the GPRB. It provides stakeholders, policymakers, and water resource managers with a graphic representation of projected future streamflow patterns under various socioeconomic situations. The graph facilitates debates and decision-making processes in the basin about water resource management, climate change adaptation, and sustainable development.

4. Comparative Analysis with Prior Studies

A thorough strategy was employed in this study to forecast future streamflow in a river basin through 2050. The process included many stages to improve dependability and accuracy.

- In the present study, three distinct bias-corrected General Circulation Models (GCMs) outputs were combined initially using a reliability ensemble averaging approach. This method not only reduced model-specific uncertainty but also increased the precision of precipitation and temperature estimates to 2050. This is a significant improvement over earlier research that frequently depended on a single GCM output [51,52], perhaps producing forecasts that were less reliable.

- Furthermore, using the Cellular Automata (CA)-Markov model to estimate future changes in land use and land cover (LULC) gave the analysis a geographical component. This technique recognized the crucial role of future land use changes in determining streamflow patterns. This differs from many past research, which mainly concentrated on meteorological variables without specifically taking the impact of changing landscapes into account [53,54]. Conventional hydrologic studies that employ hydrologic modelling software often focus on evaluating historical LULC data to forecast future streamflow [55]. However, these studies frequently encounter a drop in accuracy as they do not account for potential changes in the landscape that may occur in the future.
- The integration of LULC data with flow accumulation (FA) can enhance the accuracy of streamflow prediction models in depicting the spatial distribution of water movement and flow channels within a watershed. FA incorporates topographic characteristics and drainage patterns, while LULC data provides insights into the types and attributes of land cover. In contrast to prior research that primarily addressed climate-driven factors [53–55], this approach acknowledges the complex interplay between alterations in land use and hydrological responses.
- In the context of this work, the application of deep learning methodologies for the purpose of streamflow forecasts presents a significant benefit when compared to traditional hydrologic modelling software. The use of deep learning (DL), specifically through the implementation of Long Short-Term Memory (LSTM) networks, allows our model to effectively capture complex and non-linear connections that are inherent in hydrological processes. This is in contrast to conventional hydrologic modelling methods, which frequently need manual calibration and may encounter difficulties in adequately capturing intricate dynamics [55,56]. Deep learning models have the potential to independently acquire patterns from extensive datasets, hence enhancing their forecast accuracy and capacity to adjust to dynamic circumstances. On the contrary hand, conventional hydrologic models need substantial parameter calibration [56,57]. Hydrologic models provide beneficial insights; however, the data-driven method of deep learning allows for more flexible and data-intensive studies. This technique can reveal minor variations in streamflow dynamics, resulting in more accurate forecasts in the presence of altering hydrological circumstances.

5. Conclusions

The integrated technique of multi-GCM simulated FA-LULC overlaid streamflow projection demonstrated in this work has major implications for water resource management in the Greater Pamba River Basin and other similar locations. It provides a complete framework that integrates climate models, weighted land use/land cover information in conjunction with flow accumulation, and sophisticated deep learning approach to enhance streamflow projections. As far as we know, no prior study has implemented the FA-weighted LULC overlay in conjunction with GCM inputs for future streamflow projection. The study took into account the uncertainty related to climate change estimates by using an ensemble of GCMs. The REA method ensured that the forecast of future precipitation and temperature patterns, crucial factors in streamflow dynamics, were more accurate and representative. This ensemble-based technique offered researchers a thorough grasp of the variety of potential streamflow situations, facilitating more informed decision-making in the management and allocation of water resources.

The streamflow estimates were improved further by including flow accumulation-weighted LULC overlay. The spatial distribution of different land cover types and their effects on hydrological processes could potentially be taken into consideration owing to the overlay technique. Traditional hydrological models frequently make use of imprecise, time-invariant representations of LULC, such as land use classes or broad land cover categories. They ignore the heterogeneity that arises as a result of changes in vegetation, urbanization, or land management techniques and presume homogeneous features within these groups.

The study's use of zonal statistics increased the accuracy of streamflow estimates by capturing the impact of various land cover features within certain flow concentration zones and in temporal scale as well.

The modelling of intricate temporal dependencies and time-lag patterns in streamflow data was made possible by the use of a deep learning environment, specifically LSTM networks, which substantially improve the accuracy of streamflow predictions including the extremes of all the three stations. By accounting the past streamflow, precipitation, temperature, and statistical summaries from the LULC overlay, the DL model effectively captured the interactions between these variables and provided accurate streamflow forecasts with higher NSE values for all the scenarios of climate-LULC linked projections than that of the climate only induced projection. The incorporation of FA-LULC along with the climate parameters results in higher accuracy streamflow projections. For Kallooppara, the climate-FA-LULC integrated projection of the scenario SSP126 yields 5.11% more accuracy than climate parameterized projection. Again for SSP245 and SSP585, the projection accuracies are 2.4% and 8.3% more respectively for integrated projection.

The study establishes the merits of combining the climate-FA-LULC parameters for streamflow forecasts and it can be extended for near, mid and far future projections, to provide quantiles of predicted inundation depths at additional locations, enabling the development of flood inundation maps for the future under the influence of forecast uncertainty. The study's findings enable to establish improved decision-making processes in the basin, such as water allocation, flood prevention, and ecosystem management. Furthermore, the approach and insights acquired from this work might serve as a platform for future research and applications in hydrological modelling and streamflow forecasting.

Author Contributions: A.S. and A.N.G.R.N. conceptualized the work. A.N.G.R.N. and S.D.S. extracted and processed the data. A.N.G.R.N., S.D.S. and M.G.M. performed the implementation. A.N.G.R.N. prepared the draft. A.S. revised the manuscript. A.S. supervised the research work. All authors have read and agreed to the published version of the manuscript.

Funding: This research received no external funding.

Institutional Review Board Statement: Not Applicable.

Informed Consent Statement: Not Applicable.

Data Availability Statement: All the datasets used in this study are taken from public databases. The daily streamflow data is available from Water Resource Information System, WRIS accessed on 7 December 2020 (www.indiawris.gov.in), bias-corrected climate projection GCM data from Mishra et al., 2020, LULCs from NASA Power (<https://power.larc.nasa.gov/>) and BHUVAN NRSC (<https://bhuvan-app1.nrs.gov.in/thematic/thematic/index.php>) both accessed on 2 February 2023, daily precipitation data from IMD (https://www.imdpune.gov.in/cmpg/Griddata/Rainfall_25_NetCDF.html) accessed on 5 March 2022 and DEM from JAXA ALOS accessed on 5 March 2022 (https://www.eorc.jaxa.jp/ALOS/en/dataset/aw3d30/aw3d30_e.htm).

Acknowledgments: We would like to thank the Water Resource Information System, WRIS for providing the daily streamflow data for 3 gauge stations, Mishra et al., 2020 for providing the bias-corrected climate projection GCM data (ACCESS-ESMI-5, INM-CM5-0 and MPI-ESMI-2-HR) for different scenarios of SSP126, SSP245 and SSP585, of CMIP6, IMD for 0.25 × 0.25 resolution precipitation data, NASA Earthdata for LULC data and NASA POWER for daily maximum and minimum temperature for the selected points and JAXA ALOS for the DEM of the study area. This study is done using ArcGIS, QGIS 2.18, Excel and Python platforms. Arathy acknowledges All India Council of Technical Education (AICTE) for the Doctoral fellowship support.

Conflicts of Interest: The authors declare no conflict of interest.

References

1. Babur, S.; Gowda, R. Streamflow Response to Land-Use Land Cover change over the Nethravathi River Basin, India. *J. Hydrol. Eng.* **2015**, *20*, 05015002. [[CrossRef](#)]
2. Chen, M.; Vernon, C.R.; Graham, N.T.; Hejazi, M.; Huang, M.; Cheng, Y.; Calvin, K. Global land use for 2015–2100 at 0.05° resolution under diverse socioeconomic and climate scenarios. *Sci. Data* **2020**, *7*, 320. [[CrossRef](#)] [[PubMed](#)]
3. Sadhwani, K.; Eldho, T.I.; Jha, M.K.; Karmakar, S. Effects of Dynamic Land Use/Land Cover Change on Flow and Sediment Yield in a Monsoon-Dominated Tropical Watershed. *Water* **2022**, *14*, 3666. [[CrossRef](#)]
4. Nourani, V.; Roushangar, K.; Andalib, G. An inverse method for watershed change detection using hybrid conceptual and artificial intelligence approaches. *J. Hydrol.* **2018**, *562*, 371–384. [[CrossRef](#)]
5. Bock, L.; Lauer, A.; Schlund, M.; Barreiro, M.; Bellouin, N.; Jones, C.; Meehl, G.A.; Predoi, V.; Roberts, M.J.; Eyring, V. Quantifying Progress Across Different CMIP Phases With the ESMValTool. *J. Geophys. Res. Atmos.* **2020**, *125*, e2019JD032321. [[CrossRef](#)]
6. Halmy, M.W.A.; Gessler, P.E.; Hicke, J.A.; Salem, B.B. Land use/land cover change detection and prediction in the north-western coastal desert of Egypt using Markov-CA. *Appl. Geogr.* **2015**, *63*, 101–112. [[CrossRef](#)]
7. Zhang, Z.; Gao, J.; Gao, Y. The influences of land use changes on the value of ecosystem services in Chaohu Lake Basin, China. *Environ. Earth Sci.* **2015**, *74*, 385–395. [[CrossRef](#)]
8. Abba Umar, D.; Ramli, M.F.; Tukur, A.I.; Jamil, N.R.; Zaudi, M.A. Detection and prediction of land use change impact on the streamflow regime in Sahelian river basin, northwestern Nigeria. *H2Open J.* **2021**, *4*, 92–113. [[CrossRef](#)]
9. Mekonnen, Y.A.; Manderso, T.M. Land use/land cover change impact on streamflow using Arc-SWAT model, in case of Fetam watershed, Abbay Basin, Ethiopia. *Appl. Water Sci.* **2023**, *13*, 111. [[CrossRef](#)]
10. Hyandye, C.; Martz, L.W. A Markovian and cellular automata land-use change predictive model of the Usangu Catchment. *Int. J. Remote Sens.* **2017**, *38*, 64–81. [[CrossRef](#)]
11. Hamad, R.; Balzter, H.; Kolo, K. Predicting Land Use/Land Cover Changes Using a CA-Markov Model under Two Different Scenarios. *Sustainability* **2018**, *10*, 3421. [[CrossRef](#)]
12. López-Vicente, M.; Pérez-Bielsa, C.; López-Montero, T.; Lambán, L.; Navas, A. Runoff simulation with eight different flow accumulation algorithms: Recommendations using a spatially distributed and open-source model. *Environ. Model. Softw.* **2014**, *62*, 11–21. [[CrossRef](#)]
13. Ficklin, D.L.; Stewart, I.T.; Maurer, E.P. Climate Change Impacts on Streamflow and Subbasin-Scale Hydrology in the Upper Colorado River Basin. *PLoS ONE* **2013**, *8*, e71297. [[CrossRef](#)] [[PubMed](#)]
14. Dallison, R.J.H.; Williams, A.P.; Harris, I.M.; Patil, S.D. Modelling the impact of future climate change on streamflow and water quality in Wales, UK. *Hydrol. Sci. J.* **2022**, *67*, 939–962. [[CrossRef](#)]
15. Mahmoodi, N.; Kiesel, J.; Wagner, P.D.; Fohrer, N. Spatially distributed impacts of climate change and groundwater demand on the water resources in a wadi system. *Hydrol. Earth Syst. Sci.* **2021**, *25*, 5065–5081. [[CrossRef](#)]
16. Parajuli, P.B.; Risal, A. Evaluation of Climate Change on Streamflow, Sediment, and Nutrient Load at Watershed Scale. *Climate* **2021**, *9*, 165. [[CrossRef](#)]
17. Ismail, H.; Rowshon, M.K.; Hin, L.S.; Abdullah, A.F.B.; Nasidi, N.M. Assessment of climate change impact on future streamflow at Bernam river basin Malaysia. *IOP Conf. Ser. Earth Environ. Sci.* **2020**, *540*, 012040. [[CrossRef](#)]
18. Ismail, M.; Ahmed, E.; Peng, G.; Xu, R.; Sultan, M.; Khan, F.U.; Aleem, M. Evaluating the Impact of Climate Change on the Stream Flow in Soan River Basin (Pakistan). *Water* **2022**, *14*, 3695. [[CrossRef](#)]
19. Held, I.M.; Soden, B.J. Robust Responses of the Hydrological Cycle to Global Warming. *J. Clim.* **2006**, *19*, 5686–5699. [[CrossRef](#)]
20. Marvel, K.; Bonfils, C. Identifying external influences on global precipitation. *Proc. Natl. Acad. Sci. USA* **2013**, *110*, 19301–19306. [[CrossRef](#)]
21. Gosling, S.N.; Arnell, N.W. A global assessment of the impact of climate change on water scarcity. *Clim. Chang.* **2016**, *134*, 371–385. [[CrossRef](#)]
22. Shahi, S.; Abermann, J.; Heinrich, G.; Prinz, R.; Schöner, W. Regional Variability and Trends of Temperature Inversions in Greenland. *J. Clim.* **2020**, *33*, 9391–9407. [[CrossRef](#)]
23. Her, Y.; Yoo, S.H.; Cho, J.; Hwang, S.; Jeong, J.; Seong, C. Uncertainty in hydrological analysis of climate change: Multi-parameter vs. multi-GCM ensemble predictions. *Sci. Rep.* **2019**, *9*, 4974. [[CrossRef](#)] [[PubMed](#)]
24. Gonzalez, P.; Neilson, R.P.; Lenihan, J.M.; Drapek, R.J. Global patterns in the vulnerability of ecosystems to vegetation shifts due to climate change. *Glob. Ecol. Biogeogr.* **2010**, *19*, 755–768. [[CrossRef](#)]
25. Nourani, V.; Jabbarian Paknezhad, N.; Sharghi, E.; Khosravi, A. Estimation of prediction interval in ANN-based multi-GCMs downscaling of hydro-climatologic parameters. *J. Hydrol.* **2019**, *579*, 124226. [[CrossRef](#)]
26. Baghanam, A.H.; Nourani, V.; Keynejad, M.A.; Taghipour, H.; Alami, M.T. Conjunction of wavelet-entropy and SOM clustering for multi-GCM statistical downscaling. *Hydrol. Res.* **2018**, *50*, 1–23. [[CrossRef](#)]
27. Ahmed, K.; Sachindra, D.A.; Shahid, S.; Demirel, M.C.; Chung, E.S. Selection of multi-model ensemble of general circulation models for the simulation of precipitation and maximum and minimum temperature based on spatial assessment metrics. *Hydrol. Earth Syst. Sci.* **2019**, *23*, 4803–4824. [[CrossRef](#)]
28. Tegegne, G.; Kim, Y.; Lee, J. Spatiotemporal Reliability Ensemble Averaging of Multimodel Simulations. *Geophys. Res. Lett.* **2019**, *46*, 12321–12330. [[CrossRef](#)]

29. Cho, K.; Kim, Y. Improving streamflow prediction in the WRF-Hydro model with LSTM networks. *J. Hydrol.* **2022**, *605*, 127297. [[CrossRef](#)]
30. Kumaran, N.K.P.; Padmalal, D.; Limaye, R.B.; Jennerjahn, T.; Gamre, P.G. Tropical Peat and Peatland Development in the Floodplains of the Greater Pamba Basin, South-Western India during the Holocene. *PLoS ONE* **2016**, *11*, e0154297. [[CrossRef](#)]
31. Mishra, V.; Bhatia, U.; Tiwari, A.D. Bias-corrected climate projections for South Asia from Coupled Model Intercomparison Project-6. *Sci. Data* **2020**, *7*, 338. [[CrossRef](#)] [[PubMed](#)]
32. Tan, Y.; Guzman, S.M.; Dong, Z.; Tan, L. Selection of Effective GCM Bias Correction Methods and Evaluation of Hydrological Response under Future Climate Scenarios. *Climate* **2020**, *8*, 108. [[CrossRef](#)]
33. Hengade, N.; Eldho, T.I. Assessment of LULC and climate change on the hydrology of Ashti Catchment, India using VIC model. *J. Earth Syst. Sci.* **2016**, *125*, 1623–1634. [[CrossRef](#)]
34. Gashaw, T.; Tulu, T.; Argaw, M.; Worqlul, A.W.; Tolessa, T.; Kindu, M. Estimating the impacts of land use/land cover changes on Ecosystem Service Values: The case of the Andassa watershed in the Upper Blue Nile basin of Ethiopia. *Ecosyst. Serv.* **2018**, *31*, 219–228. [[CrossRef](#)]
35. Hunt, K.M.R.; Matthews, G.R.; Pappenberger, F.; Prudhomme, C. Using a long short-term memory (LSTM) neural network to boost river streamflow forecasts over the western United States. *Hydrol. Earth Syst. Sci.* **2022**, *26*, 5449–5472. [[CrossRef](#)]
36. Arsenault, R.; Martel, J.L.; Brunet, F.; Brissette, F.; Mai, J. Continuous streamflow prediction in ungauged basins: Long short-term memory neural networks clearly outperform traditional hydrological models. *Hydrol. Earth Syst. Sci.* **2023**, *27*, 139–157. [[CrossRef](#)]
37. Wilbrand, K.; Taormina, R.; ten Veldhuis, M.C.; Visser, M.; Hrachowitz, M.; Nuttall, J.; Dahm, R. Predicting streamflow with LSTM networks using global datasets. *Front. Water* **2023**, *5*, 1166124. [[CrossRef](#)]
38. Nifa, K.; Boudhar, A.; Ouatiqi, H.; Elyoussfi, H.; Bargam, B.; Chehbouni, A. Deep Learning Approach with LSTM for Daily Streamflow Prediction in a Semi-Arid Area: A Case Study of OumEr-Rbia River Basin, Morocco. *Water* **2023**, *15*, 262. [[CrossRef](#)]
39. Tebaldi, C.; Knutti, R. The use of the multi-model ensemble in probabilistic climate projections. *Philos. Trans. R. Soc. A Math. Phys. Eng. Sci.* **2007**, *365*, 2053–2075. [[CrossRef](#)]
40. Karimi, H.; Jafarnezhad, J.; Khaledi, J.; Ahmadi, P. Monitoring and prediction of land use/land cover changes using CA-Markov model: A case study of Ravansar County in Iran. *Arab. J. Geosci.* **2018**, *11*, 592. [[CrossRef](#)]
41. Jafarpour Ghalehtemouri, K.; Shamsoddini, A.; Mousavi, M.N.; BintiCheRos, F.; Khedmatzadeh, A. Predicting spatial and decadal of land use and land cover change using integrated cellular automata Markov chain model based scenarios (2019–2049) Zarriné-Rūd River Basin in Iran. *Environ. Chall.* **2022**, *6*, 100399. [[CrossRef](#)]
42. Beroho, M.; Briak, H.; Cherif, E.K.; Boulahfa, I.; Ouallali, A.; Mrabet, R.; Kebede, F.; Bernardino, A.; Aboumaria, K. Future Scenarios of Land Use/Land Cover (LULC) Based on a CA-Markov Simulation Model: Case of a Mediterranean Watershed in Morocco. *Remote Sens.* **2023**, *15*, 1162. [[CrossRef](#)]
43. Mondal, M.S.; Sharma, N.; Garg, P.; Kappas, M. Statistical independence test and validation of CA Markov land use land cover (LULC) prediction results. *Egypt. J. Remote Sens. Space Sci.* **2016**, *19*, 259–272. [[CrossRef](#)]
44. Hakim, A.M.Y.; Baja, S.; Rampisela, D.A.; Arif, S. Spatial dynamic prediction of landuse/landcover change (case study: Tamalanrea sub-district, makassar city). *IOP Conf. Ser. Earth Environ. Sci.* **2019**, *280*, 012023. [[CrossRef](#)]
45. Abbas, Z.; Yang, G.; Zhong, Y.; Zhao, Y. Spatiotemporal Change Analysis and Future Scenario of LULC Using the CA-ANN Approach: A Case Study of the Greater Bay Area, China. *Land* **2021**, *10*, 584. [[CrossRef](#)]
46. Alshari, E.A.; Gawali, B.W. Modeling Land Use Change in Sana'a City of Yemen with MOLUSCE. *J. Sens.* **2022**, *2022*, 7419031. [[CrossRef](#)]
47. Kamaraj, M.; Rangarajan, S. Predicting the future land use and land cover changes for Bhavani basin, Tamil Nadu, India, using QGIS MOLUSCE plugin. *Environ. Sci. Pollut. Res.* **2021**, *29*, 86337–86348. [[CrossRef](#)]
48. Hasan, M.M.; Mondol Nilay, M.S.; Jibon, N.H.; Rahman, R.M. LULC changes to riverine flooding: A case study on the Jamuna River, Bangladesh using the multilayer perceptron model. *Results Eng.* **2023**, *18*, 101079. [[CrossRef](#)]
49. Apaydin, H.; Feizi, H.; Sattari, M.T.; Colak, M.S.; Shamshirband, S.; Chau, K.W. Comparative Analysis of Recurrent Neural Network Architectures for Reservoir Inflow Forecasting. *Water* **2020**, *12*, 1500. [[CrossRef](#)]
50. Khan, M.; Khan, A.U.; Khan, J.; Khan, S.; Haleem, K.; Khan, F.A. Streamflow forecasting for the Hunza river basin using ANN, RNN, and ANFIS models. *Water Pract. Technol.* **2023**, *18*, 981–993. [[CrossRef](#)]
51. Mansfield, L.A.; Nowack, P.J.; Kasoar, M.; Everitt, R.G.; Collins, W.J.; Voulgarakis, A. Predicting global patterns of long-term climate change from short-term simulations using machine learning. *NPJ Clim. Atmos. Sci.* **2020**, *3*, 44. [[CrossRef](#)]
52. Ghosh, S. SVM-PGSL coupled approach for statistical downscaling to predict rainfall from GCM output. *J. Geophys. Res.* **2010**, *115*. [[CrossRef](#)]
53. Patterson, N.K.; Lane, B.A.; Sandoval-Solis, S.; Persad, G.G.; Ortiz-Partida, J.P. Projected Effects of Temperature and Precipitation Variability Change on Streamflow Patterns Using a Functional Flows Approach. *Earth's Future* **2022**, *10*, e2021EF002631. [[CrossRef](#)]
54. Yang, T.; Wang, X.; Yu, Z.; Krysanova, V.; Chen, X.; Schwartz, F.W.; Sudicky, E.A. Climate change and probabilistic scenario of streamflow extremes in an alpine region. *J. Geophys. Res. Atmos.* **2014**, *119*, 8535–8551. [[CrossRef](#)]
55. Sanjay Shekar, N.C.; Vinay, D.C. Performance of HEC-HMS and SWAT to simulate streamflow in the sub-humid tropical Hemavathi catchment. *J. Water Clim. Chang.* **2021**, *12*, 3005–3017. [[CrossRef](#)]

56. Malik, M.A.; Dar, A.Q.; Jain, M.K. Modelling streamflow using the SWAT model and multi-site calibration utilizing SUFI-2 of SWAT-CUP model for high altitude catchments, NW Himalaya's. *Model. Earth Syst. Environ.* **2022**, *8*, 1203–1213. [[CrossRef](#)]
57. Singh, L.; Saravanan, S. Simulation of monthly streamflow using the SWAT model of the Ib River watershed, India. *HydroResearch* **2020**, *3*, 95–105. [[CrossRef](#)]

Disclaimer/Publisher's Note: The statements, opinions and data contained in all publications are solely those of the individual author(s) and contributor(s) and not of MDPI and/or the editor(s). MDPI and/or the editor(s) disclaim responsibility for any injury to people or property resulting from any ideas, methods, instructions or products referred to in the content.